COMPARISON OF VASCULAR NETWORKS, WATER USE AND GROWTH RATES IN TWO TREE SPECIES OF CONTRASTING FUNCTIONAL TYPE

by

Erica Isele von Allmen

A thesis submitted to the faculty of
The University of Utah
in partial fulfillment of the requirements for the degree of

Master of Science

Department of Biology

The University of Utah

May 2011

STATEMENT OF THESIS APPROVAL

The thesis of **Erica Isele von Allmen**

has been approved by the following supervisory committee members:

John S. Sperry	, Chair	**Feb. 24, 2011** Date Approved
Frederick R. Adler	, Member	**Feb. 24, 2011** Date Approved
James R. Ehleringer	, Member	**Feb. 24, 2011** Date Approved

and by **Neil J. Vickers** , Chair of

the Department of **Biology**

and by Charles A. Wight, Dean of The Graduate School.

ABSTRACT

The curious pattern of metabolic rate scaling with mass to the ¾ power has been observed across organisms and has eluded biologists for nearly a century. Metabolic scaling in trees has recently attracted attention as scientists try to model ecosystem dynamics of the hydrologic cycle and the carbon cycle. In this study, we attempt to gain greater understanding about the mechanical and hydraulic principles that govern vascular networks, how water transport through these networks scale with tree size, and how water use relates to growth rates in functionally diverse ring-porous *Quercus gambelii* and diffuse-porous *Acer grandidentatum*. We parameterized a numeric network model with species-specific vascular and structural characters to predict water use and growth rate scaling with tree size. The network model currently is confined to optimal water supply. To better understand water use and growth rate patterns during variable season conditions, we measured whole-tree sapflow, conductance and growth rates over one growing season in these two species. The numeric network model did exceptionally well at predicting species-specific scaling of water use and growth rates with tree size. In addition, it accurately predicted relative water use per species. Comparison of these two sympatric species over the growing season suggested that ring-porous *Q. gambelii* has relatively stable (isohydric) water use patterns and similar growth rates to diffuse-porous A. *grandidentatum*

which has more flexible water use strategy leading to variable growth rates. These two species are able to be co-dominant in this region due to unique water use niches and vasculature. The accuracy of the numeric model predictions tested here suggest that scaling models such as these could be valuable in making ecohydrological predictions enabling the prediction of water use and growth rates with tree size and scaling this up to the stand and ecosystem level. We hope this work infusing hydraulic and mechanical constraints driving water use and growth rates of individuals within and between species contributes to better understanding of processes that effect predictions of ecosystem challenges under global change.

TABLE OF CONTENTS

LIST OF FIGURES

ACKNOWLEDGEMENTS

I would like to express sincere gratitude to John Sperry, my advisor, for his tremendous contributions of time and resources to my master's thesis. John spent countless hours helping me comprehend modeling and plant physiology. I would also like to thank my committee, Fred Adler and Jim Ehleringer, for their assistance, support, and refinement of my thesis. It has been an honor to work with all my committee members.

The collaborative efforts with Brian Enquist, from the University of Arizona, Van Savage, from University of California, Los Angeles, and Peter Reich from the University of Minnesota, were the initiation for this project.

Along this journey I have had the privilege to interact with many people who generously supported me with friendship and camaraderie, of which this list is too long to include here. This project would not have been possible without many people who helped me with field work, technical assistance, administrative issues, and general support. Henry Grover and Andy Crawl offered up endless hours of field support and delightful company even during cold and dark predawn sampling. Kevin Hultine and Susan Bush generously offered their time, expertise and supplies for sapflow instrumentation. Not only did Kevin, Susan and Henry help with my project but they were also great friends. Duncan Smith helped

tremendously, not only with measurements, but also with computer modeling, data and statistical analyses, and all kinds of technical support. Maggie Christman helped me with general laboratory and technical support. Shannon Nielsen supported me with all kinds of administrative and logistical support.

The financial support for this dissertation came from a generous grant from NSF to John Sperry (NSF-IBN-0743148). I would like to thank Brian Enquist for a significant contribution of funding for this project from NSF (NSF-ATB-0742800). Additional financial support came from the University of Utah, Department of Biology.

Finally, I would like to thank my family and dear friends for their unconditional and unending support and encouragement through this project and the adventures we call life.

INTRODUCTION

Metabolic scaling has been observed by biologists since the early 1900s (Kleiber 1932 and Bendict 1938) as a trend in which metabolic rates scale with organisms' mass to the ¾ power (Kleiber's rule). More recently West, Brown and Enquist (1997) proposed an allometric model to explain metabolic scaling not only in animals, but also in plants (Enquist et al. 1999). Their model was a major contribution to science, not only by attempting to explain this curious observation, but also in setting up a framework to analyze the role of mechanical and hydraulic drivers of plant evolution and diversity. The West, Brown and Enquist (WBE) model was critical in creating a flurry of research to determine if and how water transport and growth rates scale with plant size.

The WBE model is based on the concept that vascular supply limits metabolic rates, and therefore, the transport rate of the vascular system will determine metabolism. Their model assumes that the vascular transport rate is directly proportional to metabolism. In order to quantify the transport rate, they model vascular transport systems via allometric scaling.

The plant version of the WBE model (here forward called the WBE plant model) assumes that plant metabolism is limited by water supply. The supply of water to leaves limits stomatal conductance and the ability for a plant to obtain CO_2, the substrate for plant metabolic processes. The WBE plant model

assumes water limits photosynthesis which in turn limits metabolism, so they assume vascular (xylem) transport rate is directly proportional to plant metabolism. However, they use plant growth rates as a proxy for metabolism because it is the easiest way to integrate the net result of metabolism at the whole-plant level. In plants, the xylem network is the vascular network of interest, so the WBE plant model aims to quantify water flow through xylem. To model the xylem network they first model the space of the external branching that will contain the internal xylem vasculature. Many reasonable assumptions (mechanical and hydraulic) about plant growth lead to predictions of whole-tree conductance scaling with tree diameter. Additional assumptions about scaling of tree mass and tree diameter lead the final predictions of growth rates scaling with mass to the ¾ power.

The WBE plant model stirred up a considerable amount of controversy. Sperry et al. (2008) were some of the toughest critics of this model due to critical inaccuracies of modeling internal vascular networks in plants. In efforts to move this model and the field forward, Sperry and Enquist decided to collaborate to rectify errors and make an effective model capable of predicting the scaling of water use and growth rates with tree size. This collaboration has proved to be fruitful not only in making a more accurate metabolic scaling model for plants, but also in making a version of the model which is able to predict not only the scaling of water use and growth rates with tree size, but the relative water use values by species. The species we chose for to test the plant model have opposing

vascular function, yet they coexist in riparian habitats. These findings are presented in Chapter 1.

The most recent version of the WBE plant model predicts water use under optimal flow conditions. The habitat in which these two species coexist is often in a suboptimal condition, with plants enduring water stress. The collection of data for an entire season allowed us to analyze the scaling of water use and growth rates under optimal conditions but also analyze the effects of season on water use and how this effects growth rates in ring-porous and diffuse-porous trees. The study of water use and growth rates in these coexisting species lead to interesting findings to follow in Chapter 2. The culmination of these two chapters presents how the hydraulic architecture in trees relates to whole-tree water use and growth rates and how water use and growth rates vary depending on water supply.

CHAPTER 1

A VASCULAR NETWORK MODEL PREDICTS WATER TRANSPORT AND GROWTH RATE SCALING FOR TWO TREE SPECIES OF CONTRASTING FUNCTIONAL TYPE

Abstract

Metabolic scaling theory aims to explain the universal pattern of organism metabolic rate scaling with mass to the ¾ power. Metabolic scaling theory for plants assumes that the rate of vascular supply (Q) is proportional to the rate of biomass growth (B). Modeling how Q scales with shoot mass (M) is used to predict growth rate scaling: $B \propto M^x$. Previous analytical transport models predict x=3/4 (Kleiber's rule) as either a central tendency or as an upper limit for tree species. We tested a species-specific numerical model against direct measurements in two tree species with contrasting vascular anatomy: a ring-porous oak (*Quercus gambelii* Nutt.) and a diffuse-porous maple (*Acer grandidentatum*, Nutt.). The model was successful in predicting how Q scales with M^x, with "x" being within 10% (maple) and 3.2% (oak) of measured exponents from sapflow data. The model accurately predicted maple's 2- to 3-fold greater water use relative to oak, and the modeled Q was within 29%

(maple) and 7% (oak) of measured Q. Most importantly, both modeled and measured Q by M^x exponents averaged 5.5% of measured B by M^x exponents, confirming the basic assumption that $B \propto Q^1$. The average "x" exponent was 0.61 ± 0.039, significantly shallower Kleiber's value of 0.75 for intraspecific scaling. The accuracy of the model, both for scaling purposes as well as for predicting rates of water consumption within and between species, argues for its further refinement and wider application in ecology and ecosystem biology.

Introduction

Biologists have long recognized scaling patterns in nature between the size and shape of an organism and its functional attributes. A famous example is "Kleiber's rule" which claims that mammalian metabolic rate scales with body mass to the ¾ power (Kleiber 1932). Scaling relationships presumably result from physical constraints that point to an underlying mechanistic explanation for limitations on resource use at the organismal, ecological, and ecosystem levels (Enquist et al. 1998, Enquist et al. 1999, Niklas and Enquist 2003, Enquist et al. 2007, West et al. 2009).

West, Brown and Enquist (1997) developed a general allometric model (WBE) that is based on physical constraints of mechanical support and rates of resource delivery through vascular networks. The WBE model predicts Kleiber's rule for mammals and proposes that the same rule should apply to vascular plants. The original WBE plant model was recently improved by a more accurate representation of tree vasculature (Savage et al. 2010). The Savage et al. model ("Savage model" hereafter) differs from WBE in predicting Kleiber's rule as an

upper bound for trees, with typical trees showing less than ¾ power scaling of metabolism with mass. In this paper we test a numerical, species-specific version of the Savage model (Sperry et al. in review) against real trees of contrasting functional type and vascular structure.

There is a common logic underlying all three models (WBE, Savage, and our numerical version). Metabolic scaling is predicted from how the twin constraints of mechanical support and hydraulic supply scales with trunk diameter (D; Table 1.1 lists symbols). Mature trees are assumed to follow a power law scaling between D and tree mass (M): $D \propto M^c$, where the "c" exponent is predicted from mechanical support considerations. Similarly, approximate power scaling is assumed between the rate of vascular water transport (Q) and D: $Q \propto D^q$. The model calculates the volume of the tree and then fills this space with the xylem conduit network through which the water flows. Combining the mechanical support ($D \propto M^c$) and the hydraulic supply ($Q \propto D^q$) results in a prediction for how flow rate scales with mass: $Q \propto M^{cq}$. Vascular supply is presumed to limit metabolic rate, expressed as biomass growth rate (B), such that $B \propto Q^1$. Therefore, $Q \propto B \propto M^{cq}$.

Diameter and mass scaling (the "c" exponent: Table 1.1) is obtained by assuming strictly self-similar branching (all twigs equidistance from the root crown), DaVinci's rule (area-preserving branching across all branching levels from trunk to twig) and elastic similarity of mature trees (constant safety margin against gravitational buckling with increasing D). It has been shown theoretically and empirically that elastic similarity requires tree height (H) to scale with $D^{2/3}$

Table 1.1. Definition of symbols

Symbol	Definition
A	net assimilation of CO_2
A_{sw}	Sapwood area
B	Annual shoot biomass growth rate
B_t	Bark thickness
D	Diameter of tree trunk
D_c	Diameter of xylem conduit
D_s	Diameter of stem
F	Vessel density (#/area)
g	Gravitational constant
H	Tree height
H_c	Critical buckling height
K	Tree hydraulic conductance
K_{leaf}/K_{twig}	Leaf/twig hydraulic conductance ratio
K_x/K_{HP}	Xylem/Hagen Poiseuille conductance ratio
K/K_{shoot}	Tree/Shoot hydraulic conductance ratio
L	Vessel or branch length
M	Shoot mass
ΔP	Soil-to-canopy pressure difference
$\Delta P'$	Driving force for water transport
P_{MD}	Mid-day leaf xylem pressure
P_{PD}	Predawn leaf xylem pressure
P_{RC}	Mid-day root crown xylem pressure
ΔP_{shoot}	Shoot pressure change (P_{MD} - P_{RC})
Q	Tree water transport rate
ΔT	Temperature difference between sensors
ΔT_m	Max temperature difference between sensors
V	Shoot volume
ρ	Wood density
c	D vs. M^c scaling exponent
f	F vs. D_c^f packing function exponent
p	D_c vs. D_s^p taper function exponent
q	Q vs. D^q scaling exponent
q'	K vs. $D^{q'}$ scaling exponent
s	A_{sw} vs. D_s^s sapwood scaling exponent

(Greenhill 1881, McMahon 1973, Niklas 1994, King 1986). Actual trees tend to become elastically similar as they grow from saplings to adult size (King 1986, Niklas 1994), a phenomenon reproduced by the models. Trees also generally conform to DaVinci's rule, at least within the larger branch diameters (Richter 1970). Based on these assumptions, the volume (V) of a tree should scale as the volume of a cylinder with the diameter and the height of the tree: $V \propto D^2 H$ (Crow 1978). Substituting $D^{2/3}$ for H, and assuming $M \propto V$, mature tree diameters should scale with shoot mass to the c=3/8 power ($D \propto M^{3/8}$).

The fact that trees "grow into" an elastically similar (log-linear) allometry as they increase in size means that power-law scaling is an approximation. Smaller size ranges of trees that have not all achieved elastic similarity are predicted to have c < 3/8. The numerical model takes this size-dependent scaling into account in its prediction of c (Sperry et al. in review).

The scaling of Q with D is predicted from the scaling of whole-tree hydraulic conductance (K) with D. Hydraulic conductance is steady-state Q divided by the portion of the soil-to-leaf water potential difference that drives the water flow ($\Delta P'$; $K=Q/\Delta P'$). Tree K will be proportional to Q if $\Delta P'$ remains constant with size as assumed by the WBE and Savage models. This assumption, however, is not well supported. What does appear constant in many cases is the *total* pressure drop from soil to canopy, ΔP, which is the sum of the pressure drop required to counteract gravity ($\rho g H$, ρ = density of water, g = gravitational constant, H = tree height) and the frictional drop, $\Delta P'$: $\Delta P = \Delta P' + \rho g H$ (Mencuccini 2003, Ryan et al. 2006). Thus, as a tree grows taller, ΔP often

stays the same, but $\Delta P'$ shrinks as gravity takes a bigger portion of ΔP. This is another source of size-dependency on the approximate power-law scaling of water transport, and it is accounted for in the numerical model (Sperry et al. in review). Because of gravity, there needs to be two "q" exponents: $K \propto D^{q'}$ (geometric property with no influence from gravity) and $Q \propto D^{q}$ (gravity accounted for). Thus, $Q \propto K^{q/q'}$ (numerical model) rather than $Q \propto K^{1}$ (WBE and Savage models).

The K by $D^{q'}$ scaling is calculated from how the number and size of xylem conduits scale with stem diameter (D_s). This implicitly assumes that the tree conductance, K, which includes nonvascular flow over a very small distance in root and leaf tissues (<1mm), is proportional to the hydraulic conductance of the xylem network. The conduit diameter (D_c) is allowed to vary from trunk to twig, according to a power law "taper function" $D_c \propto D_s^{p}$, where D_s is the stem diameter and "p" is the taper exponent (a positive number). The taper function mimics the well-documented trend for conduit diameter to increase with branch diameter (Zimmermann 1983, West et al. 1997, Savage et al. 2010, McCulloh et al. 2003, Sperry et al. 2008).

The number of conduits per xylem area (F) is allowed to vary inversely with conduit diameter according to a power law "packing function" $F \propto D_c^{f}$, where "f" is the packing exponent (a negative number). The packing function quantifies a long-recognized anatomical pattern (Baas 1986) showing that the larger the conduits are, the fewer there are per unit area, so as to occupy an approximately constant fraction of the wood area. An important contribution of the Savage

model was the incorporation of the packing function to replace the constant F across branch levels assumed by WBE (Savage et al. 2010) with increasing F with decreasing branch diameter. Hydraulic conductance of the xylem conduits is assumed to be proportional to the Hagen-Poiseuille (K_{HP}) value for ideal capillaries ((conductance/area) = $(F\pi D_c^4) / (128\mu L)$; where F is the number of conduits per area, D_c is conduit diameter, μ is the viscosity of water, and L is the length of the conduit). Although xylem tubes are connected by end-walls and hence are not ideal capillaries, there is evidence that their conductance is proportional to the Hagen-Poiseuille value (Wheeler et al. 2005, Zimmermann 1983, Gibson et al. 1984, Calkin et al. 1986). The numerical model includes a proportionality factor that accounts for the additional flow resistance of conduit end-walls (Sperry et al. in review; Methods).

The WBE and Savage predecessors modeled stems as solid cylinders of conducting xylem without radial taper or variable sapwood (actively conducting xylem); simplifications that facilitated analytical solutions. An important advance of the numerical model is the incorporation of nonconducting heartwood, bark, and pith, and the radial tapering of xylem conduits from pith to cambium, which mirrors the axial taper from trunk to twig. Incorporating these features provides a more accurate estimate of the area of sapwood as a function of branch diameter (D_S), and hence better estimates of the hydraulic conductance of the branch network.

All three models (WBE, Savage, and the numerical version) explicitly calculate only the hydraulic conductance of the branched stem network. Missing

is the contribution of the leaves and root system. Simplifying architectural patterns, like the packing and taper functions of stem xylem, are not well characterized for calculating leaf and root conductance from vascular properties. The WBE and Savage models assume implicitly that the conductance of these missing components scales isometrically with shoot conductance. The numerical version also makes this assumption, but provides explicit proportionality factors for obtaining leaf conductance from subtending twig conductances, and whole-tree conductance from shoot conductance. The greater realism of the numerical model allows it not only to predict the scaling of K and Q with D, but also the absolute values within a species and relative values between species.

The prediction of K by $D^{q'}$ scaling provides the Q by D^{q} relationship, and the major assumptions that $B \propto Q$ and $D \propto M^{c}$, leads to the scaling of growth rate (B) with mass: $B \propto M^{cq}$. The rationale for $B \propto Q$ is that water loss and CO_2 uptake occur through the same diffusion path at the stomatal pores. As long as the rate of photosynthesis is predominately limited by CO_2 diffusion (rather than by reaction kinetics), the rate of transpiration (Q) through the stomata should on average be proportional to the rate of CO_2 uptake through the same openings, and hence to net carbon assimilation. This relationship has been confirmed experimentally (Hubbard et al. 2001). If net carbon assimilation is proportional to biomass growth rate (B), then B should be proportional to Q on average. In reality, assimilated carbon is allocated to a diverse array of sinks, so this assumption is very bold. None of the three models explicitly specifies carbon

allocation, so only the scaling of B is predicted, not the absolute value or relative value between species.

The prediction of Kleiber's ¾ power rule requires that $B \propto M^{cq = 3/4}$. If "c" is approximately 3/8 (from elastic similarity), then q would have to equal 2, and tree water use would have to be proportional to tree basal area ($Q \propto D^{q = 2}$). In the WBE and Savage models where $K \propto Q$, this also means that tree conductance is proportional to basal area ($K \propto D^{q' = 2}$). At first glance, this would appear to be impossible, since by the Hagen-Poiseuille equation, hydraulic conductance for a given conduit diameter (D_c) is proportional to the number of conduits (and hence, to D^2), but also inversely proportional to length, such that $K \propto D^2/H$. However, conductance is also proportional to conduit diameter to the fourth power (D_c^4), and following the taper function, D_c becomes smaller moving from trunk to twig. Hence, the distal, narrower tubes can become a more dominant determinant of tree conductance than the path length. If the taper exponent, p, is large enough, and if the path length is long enough, tree conductance ultimately can become independent of path length (H) and scales with basal area ($K \propto D^{q' = 2}$).

The WBE and Savage models predict Kleiber's rule by solving for the minimum "p" which yields q = 2 at the limit of an infinite path length. This "p" is 1/6 for the WBE model with constant conduit number per area (F), and p = 1/3 for the Savage model where F is predicted from the packing function. In reality, trees are not infinitely tall, a fact which reduces the distal constricting effect on their hydraulic conductance. As a result, the Savage model predicts that realistic trees will have a $q \approx 1.85$ rather than q = 2 for a taper of p=1/3. Thus, the Savage

model predicts that $B \propto M^{0.69}$, in contrast to the original prediction by West, Brown, and Enquist that $B \propto M^{0.75}$. The Savage model presents Kleiber's rule as an upper limit to metabolic scaling rather than a central tendency. In the numerical model, which accounts for gravitational effects ($Q \propto K^{q/q'}$, $q < q'$), predictions of q are even lower, and Kleiber's rule is never attainable if $B \propto Q$ (Sperry et al. in review).

Although some underlying concepts and over-arching predictions of the WBE model has been tested with varying results (Enquist and Niklas 2001, Mencuccini 2003, Sperry et al. 2008, Reich et al. 2006, Makarieva et al. 2008) it is not a species' specific model, and the tests are potentially confounded by interspecific variation. The Savage model has the potential to incorporate species-specific predictions, but these would not be derivable analytically. Therefore, the development of a species' specific numerical model, which can predict both absolute values of K and Q, as well as the intraspecific scaling of K, Q and B with size (Sperry et al. in review), enables rigorous testing of the logic and concepts that underlie all three models.

To test the robustness of the numeric model across the extremes of angiosperm vascular architectures, we chose two tree species that coexist in the same habitat but represent contrasting functional groups: ring-porous oak (*Quercus gambelii*) and diffuse-porous maple (*Acer grandidentatum*). These species compete for resources in the same habitat while employing different approaches to using water and avoiding water stress. Oak vasculature has few large vessels (~50-200 μm) primarily in the early wood and conducts xylem only

in the current year's growth ring, while maple has numerous small vessels (~25-60 μm) throughout its rings and conducts xylem across multiple growth rings. We parameterized the model with species-specific inputs to calculate c and q for the size ranges of trees studied, obtaining predictions of $D \propto M^{c}$, $K \propto D^{q'}$, $Q \propto D^{q}$, and $B \propto M^{cq}$.

We tested the model on the same population of trees used for its parameterization. We measured: 1) whole-tree sapflow (Q) to get an empirical q exponent from Q by D^{q} scaling, 2) ΔP to get tree K by $D^{q'}$ scaling, 3) M by D scaling to get an empirical "c" exponent, 4) from q and c an empirical $Q \propto B \propto M^{cq}$ relationship, and 4) shoot biomass growth rates from tree cores to obtain a direct scaling exponent for $B \propto M^{x}$. The main questions we strive to answer are: 1) Are basic model assumptions of DaVinci's rule, elastic similarity, and size invariant ΔP valid? 2) How well does the model match measured whole-tree conductance and sapflow rates? 3) How well does the model match the empirical c and q scaling exponents and hence the empirical $B \propto M^{cq}$ scaling estimate? 4) Does the empirical $B \propto M^{cq}$ estimate agree with direct estimates of $B \propto M^{x}$? 5) Is $B \propto Q$ as assumed by the model?

Methods

Study site

Red Butte Canyon Research Natural Area (RNA) is the study site located approximately 8 km east of Salt Lake City, Utah at 40° 47′ latitude and 111° 48′ longitude with an elevation range from 1530 to 2510 m. Red Butte Canyon

receives roughly 500 mm of rain annually (Ehleringer et al. 1992). Study trees were selected along the riparian corridor with full canopies in the sun and as part of tree stands. Isolated trees were avoided. A riparian habitat was chosen to avoid effects of soil moisture stress that could influence ΔP and K independently of tree size.

Regression analyses

Numerous power functions were used to describe relationships between variables. These were obtained by linear regression through log-transformed data. Following the explicit advice of Warton et al. (2006), we used ordinary least squares (OLS) regression when the purpose was to predict a specific "y" value from a given "x" value. We used reduced major axis (RMA) regression when the purpose was to estimate the slope of the relationship (the scaling exponent).

Numerical model inputs

The numerical model is described in detail elsewhere (Sperry et al. in review). Inputs were obtained from trees at the study site. The model was written in Excel Visual Basic for Applications and is available from the second author on request.

External branching parameters. The tree's branching structure was specified by the same branching rules used in the Savage model: a) twig lengths and diameters are size-invariant within a species, b) all branches within the same level are equal in length and diameter, c) there is a constant ratio of daughter branches per mother branch (assumed here to be 2), d) branch lengths increase

by a constant ratio moving from daughter to mother branch levels (assumed to be 1.26), and e) branch diameters increase by a constant ratio moving from daughter to mother levels (assumed to be 1.41 in order to comply with DaVinci's rule). Assumptions d and e together result in branch length proportional to branch diameter to the 2/3 power. When trees of increasing size are built according to these rules, the tree converges on elastic similarity and tree height becomes proportional to trunk diameter to the 2/3 power.

We evaluated whether our species converged on elastic similarity with increasing branch size and also if they complied with DaVinci's rule. An oak (D=1.35 cm) and maple (D=2.83 cm) were collected from the riparian corridor in Red Butte Canyon RNA. The diameter of each stem section (between branching points) was measured at every branching point from trunk to twig tip. The corresponding maximum path length from each stem was measured from the most proximal junction to the most distant twig tip. Convergence on elastic-similarity within trees was evaluated from the allometry between stem diameter and distance from the diameter measurement to the furthest twig tip. Area-preservation was analyzed by comparing mother (proximal) and daughter (distal) stem areas at all branching points.

Compliance with elastic similarity was also evaluated across trees of the size range used for the sapflow measures (D=4-26 cm). We measured trunk diameter above the root crown (D) and maximum height (H) for the sapflow trees as well as additional ones of the same size range (maple n = 64, oak n = 51) in stands along the riparian corridor. Maximum tree height was measured with a

clinometer, sighting to the topmost point on the tree canopy, then the height was geometrically calculated with the angle from the observer to the tree top and the observer's distance from the trunk. An RMA regression of the logged H and D data gave the scaling exponent which should be 2/3 for elastic similarity.

Although the model assumes that diameter and length of the twigs are invariant with size, the twig properties can differ between species and need to be specified. Average twig diameter was determined from the same trees measured for the evaluation of DaVinci's rule. The corresponding twig length was specified to produce modeled trees with the observed average safety factor from Euler buckling for each species. Safety factors were determined from the H and D data set. The critical height (H_c) at which a tree will buckle under its own height was estimated from D using data and equations in Niklas (1994). Safety factors from gravitational buckling were computed as H_c/H for each tree in the data set.

Internal vascular parameters.The packing and taper functions. Xylem (vessel) architecture changes both radially (pith to bark) and axially (trunk to twig) within a plant. The number of vessels is related to the size of the vessels via the packing function and vessel size is related the external branch size via the taper function. Both the axial and radial functions of each relationship were assessed separately.

To obtain empirical packing and taper functions across branching levels, xylem vessel diameter and number per area were measured on transverse sections. Three oak trees (basal D=9.2, 10.5, & 11.1 cm) ranging from 26-30 years old and two maples (basal D= 11.1 & 12.3 cm) ranging from 40 to 71 years

old were cut in cross-section at four incremental branching levels from trunk to twigs (trunk, primary branching, secondary branching and twigs).

To measure vessel sizes in both axial and radial directions, two to three portions per cross-section were removed from the stem and thin (19 μm) transverse sections were cut using a sliding microtome (Reichert-Jung Optische Werke, Vienna, Austria). These sections were imaged with a digital camera mounted to a light microscope (Nikon Eclipse E600, Japan). Sections were inspected from the center of the pith to the bark. Within each sliced section, radial sector polygons, or areas of interest (AOI), were selected between rays within growth rings. For stems with <19 rings, all rings were analyzed from cambium to pith. For stems with >20 rings, consecutive rings were analyzed for the six most current rings and in the three rings closest to the pith; otherwise, every fifth ring was sampled. Ring thickness was measured for all rings from cambium to pith. In each AOI, vessel lumen area and number were quantified using Image-Pro. Vessel areas were converted into area-weighted diameters (average vessel area in a given AOI converted to vessel diameter). Area-weighted diameters were used to most accurately represent the proportion of wood area occupied by vessels. The number of vessels per AOI gave the vessel density (F; vessels per mm^2).

Linear regressions of log-transformed vessel density (F) and area-weighted vessel diameter (D_c) gave species-specific packing functions ($F \propto D_c^f$), where "f" is the packing exponent. Because the model uses the packing function to predict vessel number from vessel diameter, OLS regression was used. Axial

packing functions compared vessel density and diameter across all branching levels within the current ring, while radial packing functions pooled all data across branching levels and across rings within a branching level. There were no significant differences in axial or radial packing functions between individuals, so individual data was pooled to obtain the corresponding functions for each species.

Linear OLS regressions of log-transformed vessel diameter (D_c) and stem diameter (D_s) gave species-specific taper functions ($D_c \propto D_s^p$), where "p" is the taper exponent. The axial taper function compared stem diameter to vessel diameter from only the current year's ring across all branching levels, while the radial taper function pooled all data across branching levels and across rings within a branching level. The stem diameters for radial taper were estimated by summing ring widths from pith to each measured ring, adding the pith diameter and the estimated bark thickness (from within tree bark and stem diameter scaling, see below). There were no significant differences in axial or radial taper functions between individuals, so individual data was pooled to obtain the corresponding functions for each species.

To analyze interspecific differences in axial and radial packing and taper functions, homogeneity of regression slopes was performed in SPSS (SPSS, Inc. 1986, version 10). A standard t-test was used to test slopes between species.

Pith and bark parameters. The Savage model assumes stems are solid cylinders with pith and bark tissues (bark = phloem plus periderm) constituting a constant fraction of stem area independent of plant size. The numerical model

(Sperry et al. in review) determines how xylem area scales with stem diameter using inputs of pith and bark dimensions. Average pith diameter was determined from twig measurements in the experimental trees mentioned above. Bark thickness (B_t) was measured at each branching level in the trees used for the taper and packing functions (above). An OLS regression through log-transformed data yielded a best-fit power function for predicting B_t from branch diameter (D_s).

Sapwood function. The numerical model accounts for the fact that not all of the xylem area is sapwood, which we define as wood that is functioning in water conduction. Sapwood functions related sapwood area (A_{sw}) to stem diameter ($A_{sw} \propto D_s^s$), where "s" is the sapwood exponent. An OLS regression of log-transformed A_{sw} and D_s data was used to obtain predictions of A_{sw} from D_s for the model. The sapwood area was determined from cores taken from the sapflow trees (below). In the ring-porous oak, the majority of the water was assumed to be transported in the outermost ring of earlywood vessels. This was confirmed by dye perfusions during oak sapflow sensor calibrations (below). In maple, sapwood area was determined from in situ dye perfusions described in the sapflow methods (below).

Calculations of stem network hydraulic conductance (K_s). The taper and packing functions, together with sapwood, pith and bark functions, allowed the model to compute the number and diameter of xylem conduits with respect to axial distance from trunk to twig, and with respect to radial distance from pith (or inner sapwood radius) to cambium (Sperry et al. in review). The hydraulic conductance of the sapwood in each branch segment was calculated by

integrating from the inner sapwood radius (or pith boundary) to the cambium, using the Hagen-Poiseuille equation (viscosity = 0.001 Pa s for a 20° C sap temperature). Branch conductances were summed within a rank to give the total branch rank conductance in parallel, and the conductances across ranks in series was computed to obtain the stem network hydraulic conductance. To correct for the added hydraulic resistance of end-walls in the xylem, we used the data of Hacke et al. (2006) which reported an average 0.56 ± 0.02 fraction of xylem conduit resistance was attributed to end-walls (n=29 species, ring and diffuse-porous, including our two study species). Thus, the true xylem conductance (K_x) was obtained by multiplying the Hagen-Poiseuille conductance (K_{HP}) by the K_x/K_{HP} ratio of 0.44 (0.44=1-0.56) to correct for end-wall resistance.

Leaf-to-twig conductance ratio (K_{leaf}:K_{twig}). The hydraulic conductance of the leaf vasculature is not calculable from branch system structure and anatomy functions. Instead, the numerical model calculates the leaf conductance ratio from twig leaf conductance (K_{leaf}, all leaves on a twig in parallel) and the conductance of the supporting twig (K_{leaf}:K_{twig}). This ratio was experimentally determined for both species. Large branches (D~2-3 cm) were cut from trees in the field and brought to the laboratory in plastic bags to minimize dehydration. In the lab, current year twigs with leaves intact were cut from the larger branches underwater and fixed to tubing filled with 20 mM KCl in distilled water. Leaves were incised with a razor blade between each of the “watersheds” fed by secondary veins to expose the veinlets. Exposing the minor veins insured that the conductance measurement would largely reflect the vascular network of the

leaves and not flow through nonvascular tissue. To remove native emboli, twigs with leaves attached were submerged in the KCl solution and placed under a partial vacuum (ca. -85 KPa (gauge)) for an hour. The hydraulic conductance of the twig plus leaf vasculature was measured using the vacuum method of Kolb et al. (1994). Following this measurement, the leaves were excised at the base of the petiole, and the hydraulic conductance of the denuded twig (K_{twig}) was measured by the same method. The hydraulic conductance of all the leaves in parallel (K_{leaf}) was determined by subtracting the flow resistance of the twig without leaves from the flow resistance of the twig plus leaves. Five twigs per species were measured to obtain species averages for K_{leaf}/K_{twig}.

Tree-to-shoot conductance ratio ($K:K_{shoot}$) and mid-day soil-canopy pressure difference (ΔP). Like leaf conductance, the root conductance is not calculable from branch system anatomy. Instead, the numerical model calculates the whole-tree conductance (K, root and shoot system in series) from its ratio to shoot conductance ($K:K_{shoot}$). This ratio was approximated from the ratio of the shoot pressure drop to the soil-canopy pressure drop ($\Delta P_{shoot}/\Delta P$).

Xylem pressures were measured at roughly 10-day intervals over the growing season on the sapflow trees. Pressures were measured on excised leaves (n=3 per reading) with a Scholander pressure chamber (PMS Instruments Co., Corvallis, Oregon). On a given date, up to three pressure measurements were made for each tree: predawn pressures were taken from leaves near ground level ($P_{PD,}$ 0400-0600 hr, assumed to approximate soil water potential in the rooting zone), mid-day canopy pressure from canopy leaves in full sun (P_{MD};

1100-1400 hr), and mid-day root-crown pressure from leaves attached to the root crown (P_{RC}). To measure P_{RC}, we covered all leaves on shoots attached near the root crown with foil to allow xylem pressures to equilibrate with the root crown pressure for one hour. Covered leaves were then cut and immediately measured in the pressure chamber. Because of limitations on the number of shoots available for P_{RC} measurements, we could only measure P_{RC} on a subset of measurement days.

For days when P_{PD}, P_{RC}, and P_{MD} were measured on the same trees, we estimated $\Delta P_{shoot}/\Delta P$ from $(P_{RC}-P_{MD})/(P_{PD}-P_{MD})$. As reported in the results, this ratio was invariant with size, as was ΔP. The $\Delta P_{shoot}/\Delta P$ ratio was multiplied by K_{shoot} to give K. The $Q=K\Delta P'$, where $\Delta P'$ is the pressure drop associated with Q: $\Delta P' = \Delta P - 0.009781\ H$, where P is in MPa, and H is tree height in meters, and the constant is ρg in MPa/m.

Model outputs and bootstrapping. The modeled tree mass (M), conductance (K) , and mid-day sapflow (Q) were outputted for the same trunk diameter (D) range used to test the model, and the D by M^c, K by $D^{q'}$, and Q by D^q exponents determined. The model inputs described above all contain uncertainty. We used bootstrapping to propagate uncertainty for the most important inputs into the model output of the K and Q by D scaling. Data sets for the taper, packing, sapwood area, and K_{leaf}/K_{twig} inputs were all sampled with replacement to obtain 1000 estimates of input parameters, a process termed "bootstrapping". These four inputs were bootstrapped because based on previous analysis (Sperry et al. in review) they were found to be important for

influencing the model output. Values were drawn from these input distributions at random to parameterize the model and generate a distribution of K by $D^{q'}$ and Q by D^{q} exponents and intercepts (n = 1000 model runs). The 95% confidence interval for the q', q, and c·q distributions (where c was assumed without error) were computed as the 2.5th and 97.5th percentile of the distribution. The bootstrapped distributions were approximately normal, so their percentile-based confidence intervals are comparable with 95% intervals estimated for measurements of q' and q.

Measuring whole-tree sapflow (Q) and whole-tree conductance (K)

Whole-tree Q and K were measured across a range of tree diameters from Red Butte Canyon RNA (oak D: 4-23 cm, maple D: 5-26 cm). The upper diameter range approached the maximum for this riparian forest. Three study locations (1660 m, 1680 m, 1730 m) were chosen along the riparian corridor. These sites were selected to have similar stand structure (continuous stands without isolated individuals). At each site, 12 trees were selected with upper canopies in full sun. Across sites there was a total 18 individuals from each species.

Temperature and percent relative humidity were measured (HMP35C, HMP50, CS500; Campbell Scientific, Logan, Utah) at each of three locations every 30 seconds and averaged and stored every 30 minutes in dataloggers (CR7X; Campbell Scientific, Logan, Utah) from June through October 2009. The air temperature and relative humidity were used to calculate atmospheric vapor pressure deficit (VPD). Photosynthetic active radiation (PAR) was measured with

a LI-COR quantum sensor (LI-190SZ, LI-COR Biosciences, Lincoln, Nebraska) every 30 seconds and averaged every 30 minutes by a datalogger (CR10X; Campbell Scientific, Logan, Utah) roughly 1 km away at an existing weather station in Red Butte Canyon. Daily precipitation was measured at this site using a tipping-bucket rain gauge (TE525; Campbell Scientific, Logan, Utah).

Whole-tree water use (Q). The rate of water transport (Q) was measured at each tree using heat dissipation sensors (Granier 1985). Granier sensors yield the temperature difference (ΔT) between a constantly heated downstream sensor and an unheated, reference sensor located upstream. Paired sensors were inserted 15 cm apart (axially) on random sides of the tree trunk at breast height. Standard Granier probes (20mm long) were used in maples, while shorter probes (10mm long) were used for oaks due to their shallow active xylem layer. Sap flowing past the heated sensor dissipates heat and reduces ΔT. The ΔT relative to the maximum value at zero flow (ΔT_m) is empirically related to the sapflow per sapwood area $Q/A_{sw}=a((\Delta T_m/\Delta T)-1)^b$. Parameters a and b are best-fit values. The ΔT was measured every 30 seconds and averaged every 30 minutes using dataloggers (CR7X, Campbell Scientific, Logan, Utah) from full leaf out until leaf senescence (June 15-Oct 31, 2009).

Recent tests have validated Granier's original calibration, where a=0.119 mm/s and b=1.23 for diffuse-porous species (20 mm probes) growing in the Salt Lake City area, but indicate that new calibrations are necessary for ring-porous species (Bush et al. 2010, Wilson et al. 2001). Because of this, we used Granier's intercepts for maple but calibrated the oak. Calibrations were

performed according to Bush et al. (2010). Six oak trees were cut (~4 m in length) then cut again underwater (~1 m in length) and kept moist in plastic bags while transported to the lab where 10 mm sensors were installed. One end of the trunk (5.5-7.8 cm diameter between sensors) was placed in tap water on an electric balance. The other end of the trunk was connected to a vacuum to induce a physiological range of pressure differences and sapflow rates. For each pressure difference, the ΔT was logged every 30 seconds and averaged every minute on a datalogger (CR10x, Campbell Scientific, Logan, Utah) while Q was measured by water uptake from the balance. After the flow data was gathered, Safranin O dye solution (0.1%) was perfused to stain the sapwood, and sapwood area (A_{sw}) was measured to determine sap flux density (Q/A_{sw}) during the experiment. An OLS regression between $(\Delta T_m/\Delta T)-1$ and sapflow density yielded intercept *a* and exponent *b* for the 10 mm probes. The oak calibration gave *a*=7.17 mm/s and *b*=1.33.

To obtain whole-tree sapflow (Q) from sensors in the field, sapwood area was measured from each experimental tree, using a 12 mm increment borer (Haglöf, Sweden). From each tree, cores were collected between sensors. In oak, conducting sapwood area was estimated by measuring the area of the current year's earlywood. To determine actively conducting sapwood area in maples, holes were drilled under water into the center of the trunk and injected with 0.1% Safranin O dye. This was performed at mid-day only on full sun days. Cores were taken from the height between the sensors (10 cm above the dye injection site) after trees had transpired dye for 1 hour. The dyed sapwood depth

was used to calculate the conducting sapwood area (A_{sw}). Clearwater correction (Clearwater et al. 1999) was applied to any maple probe that exceeded the depth of sapwood. Sapflow (Q) was calculated for each tree by multiplying sapflow density and sapwood area ($Q=Q/A_{sw} * A_{sw}$).

We report Q for mid-day time periods which correspond to our measurements of ΔP (below). Mid-day Q was the average of the top 5 daytime values (each a 30 minute mean). The model predicts Q only under well-watered conditions where it is limited by stomatal regulation of canopy xylem pressure rather than by low light, soil moisture, or VPD. Therefore, we did not use Q data from cloudy days, or from periods where predawn xylem pressures became more negative, which indicated soil drought. To filter low VPD periods we plotted Q for each tree versus the corresponding day's mean VPD. All Q data below the top 10% VPD range were excluded.

Tree conductance (K) was calculated by dividing Q by mid-day pressure difference with the gravitational drop subtracted ($K= Q/\Delta P'$) for each tree. To estimate $\Delta P'$ ($\Delta P' = \Delta P - 0.009781$ H) for each day, ΔP was interpolated between ΔP measurement days. Daily $\Delta P'$ per tree was used to calculate daily K, and K's were averaged over the sampling dates. Mean whole-tree conductance was compared to tree diameter to obtain $K \propto D^{q'}$ using an RMA regression.

Scaling of aboveground (shoot) mass (M) with tree size (D)

Tree height (H) by diameter (D) data (explained above) combined with wood density measurements were used to determine exponent c, how mass scales with tree diameter ($D \propto M^c$). By modeling trees as cylinders per DaVinci's

rule, we estimated the volume of each tree (V; $V = \pi/4\ D^2\ H$). Combining tree volume with measurements of wood density (ρ, dry weight/fresh volume) yielded aboveground tree mass (M; $M = V\ \rho$) for each trunk diameter, D. Log-transformed data of D and M were fit with an RMA regression to estimate the $D \propto M^c$ scaling exponent (c).

Wood density was determined from the mean of 6 tree cores at breast height (~1 cm wide by 4 cm deep) and 6 branches (~4 cm long by 1 cm diameter) per species. Fresh volume was calculated from the weight of water displaced as wood samples were submerged in water on an electric balance (Archimedes principle). The segments were place in a 60° C oven for 14 days then removed and weighed again. Density was expressed as ρ= dry weight / fresh volume in g/cm^3.

Empirical scaling of shoot biomass growth rate (B) with mass (M^x)

Aboveground biomass accumulation (B) was estimated from radial cores taken from trees at breast height. Trees were the same 36 individuals (18/species) used in sapflow measurements. Cores allowed us to reconstruct the relationship between D and year for each tree, which we converted to M vs. year using the OLS height and diameter allometry and wood density data. From these data, the annual shoot mass increments, $B = \Delta M/year$, were calculated over the life of each experimental tree and plotted vs. M. For each tree, an RMA regression was run through the log-transformed data, then all RMA slopes were averaged to yield a mean exponent for B by M^x scaling per species.

The empirical B by M exponent “x” should be equal to empirical values of c times q if $B \propto Q$ as assumed by metabolic scaling theory. We used bootstrapping to propagate uncertainty in the c and q estimates to their product in order to compare it with the B by M exponent x. The H by D data set and the Q by D data set were each sampled with replacement to generate 1000 estimates of c and q. Values were drawn from these estimates at random to generate a distribution of the product c and q (n=1000), and the 95% confidence interval computed as the 2.5th and 97.5th percentile of the distribution.

Statistics

Standard “t” tests (P=0.05) were used to compare empirical means or regression intercepts between species, and to compare measurements with parametric values (e.g., values without error). The “t” test could not be used with the bootstrapped distributions (modeled exponent q, c·q, and measured c·q) because the “sample size” was arbitrary. In the case of comparing measured c·q, and x, we used two methods for comparing the distributions: log likelihood and overlap. To compute log likelihood values, we fit a continuous probability density function to each of the two distributions. The log likelihood for each distribution was computed as the sum of the logged probability densities for each “x” observation (n=18 trees per species). Generally, statisticians have suggested that likelihood values within two units of each other are considered similar (Edwards 1992). To compute the overlap between the two probability density distributions, we integrated their overlapping area. The more similar the distributions, the greater their fraction of overlap (0-1; 1 = same distribution). We

did not compare the modeled c·q distribution using these methods because model output lacked measurement error and its distribution was expected to be narrower than measured distributions. Thus, even if the mean model prediction was exactly the same as the measured mean, log likelihood and % overlap metrics would indicate dissimilar distributions.

Results

Model inputs and assumptions

Model inputs are summarized in Table 1.2. Most were straight forward (twig diameter and length, pith/twig diameter, bark thickness, and sapwood areas), but some require more explanation.

DaVinci's rule, elastic similarity, and safety margins from buckling. DaVinci's rule was supported from comparisons of mother and daughter cross-sectional branch areas. For mother branch diameters above 7 mm, mother/daughter areas did not differ from the expected ratio of one in both species (Fig. 1.1; maple mother/daughter = 1.01 $\pm$ 0.02; oak mother/daughter=0.97 $\pm$ 0.09; mean $\pm$ SE). However for smaller branches (<7 mm), "t" tests indicate that the mother/daughter ratio was greater than one. This probably resulted from twig dieback which was prevalent in the study site. Within tree relationships between stem diameter (D_s) and maximum distal path length showed the expected convergence on elastic similarity as D_s increased (Fig. 1.2, solid symbols). This is consistent with the assumptions of the model that individual stem segment length scales with $D_s^{2/3}$. Elastic similarity (dotted

Table 1.2. Summary of model inputs. Means are given with standard errors except for twig length, which was chosen to yield buckling safety factors matching observed values. Those inputs in the form of power functions were determined from OLS regressions of logged data. See Table 1.1 for definition of symbols.

Model input Parameter	**maple**	**Oak**
twig diameter (mm)	1.36 ± 0.025	1.83 ± 0.089
twig length (mm)	105	98
pith diameter/twig diameter	0.519 ± 0.013	0.351 ± 0.029
bark thickness: B_t (mm), D_s (mm)	$B_t = 0.046\ D_s^{1.05}$	$B_t = 0.85\ D_s^{0.64}$
buckling safety factor H_c/H	2.61 ± 0.06	3.38 ± 0.11
sapwood area: A_{sw} (mm^2), D_s (mm)	$A_{sw} = 0.787\ D_s^{1.86}$	$A_{sw} = 0.067\ D_s^{1.21}$
packing function: F (mm^{-2}), D_c (μm)	$F = 4.61 \times 10^4\ D_c^{-1.62}$	$F = 1.28 \times 10^4\ D_c^{-1.39}$
taper function: D_c (μm), D_s (mm)	$D_c = 13.77\ D_s^{0.145}$	$D_c = 15.52\ D_s^{0.385}$
K_x/K_{HP}	0.44	0.44
K_{leaf}/K_{twig}	0.38 ± 0.038	0.27 ± 0.065
ΔP, MPa	1.29 ± 0.03	1.32 ± 0.04
K/K_{shoot}	0.57 ± 0.07	0.84 ± 0.03

line) was confirmed across trees of the size used to determine sapflow scaling (D = 4-35 cm). In both species, height and diameter relationships had scaling exponents (from RMA regressions) that were not significantly different from 2/3 (Fig. 1.2, open symbols, maple exponent=0.64, 95% confidence interval: 0.57-0.71, oak=0.69: 0.59-0.80). Safety factors from buckling (H_c/H; Fig. 1.2, arrows) averaged 2.61 ± 0.06 in maple and 3.38 ± 0.11 in oak, these were also required as model inputs required to set twig length (Table 1.2).

Packing and taper functions. In maple, a test of homogenous regressions of log-transformed data showed the axial packing exponent and intercept were significantly different from the radial values (Fig. 1.3). In oak, axial and radial functions were not different (Table 1.2, Fig. 1.3). Because the model can only accept a single packing function as an input, the pooled function was used for

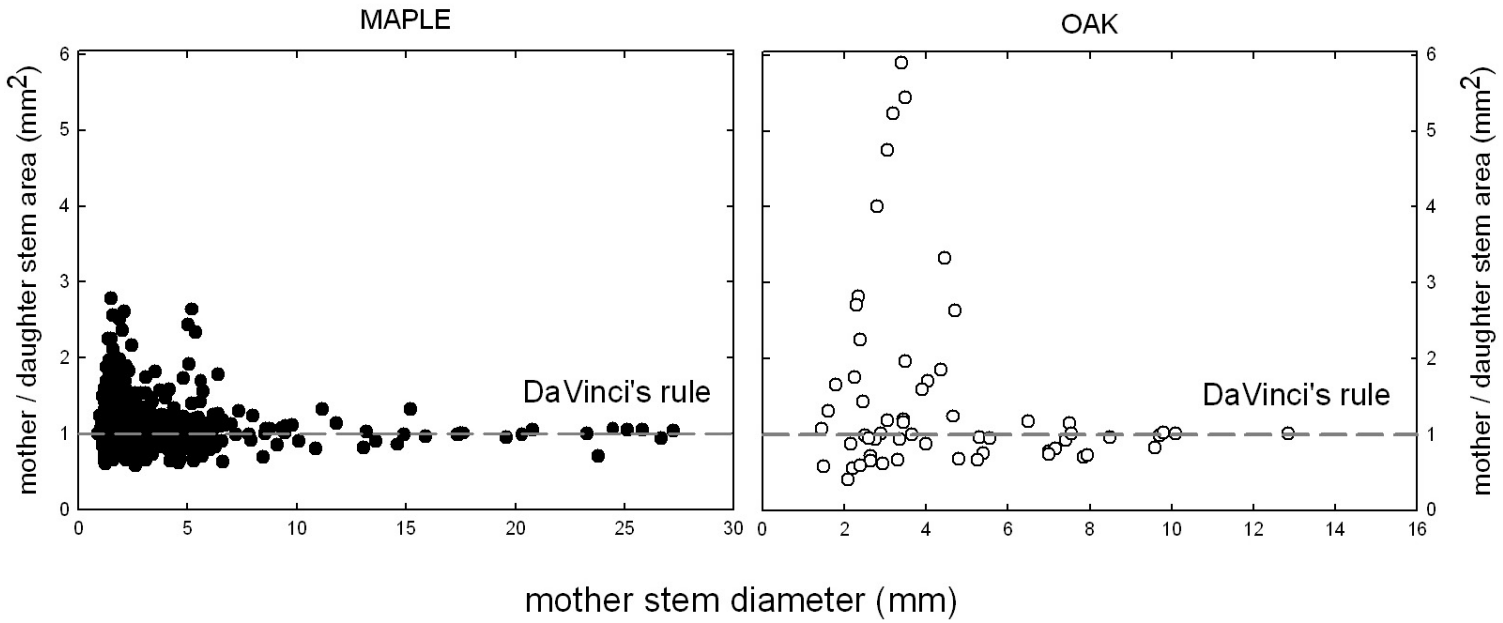

Figure 1.1. Comparison of mother stem diameter (mm) and mother/daughter stem area ratio in oak (open symbols) and maple (closed symbols). Da Vinci's rule (dashed line) gives a mother/daughter stem area ratio of 1.

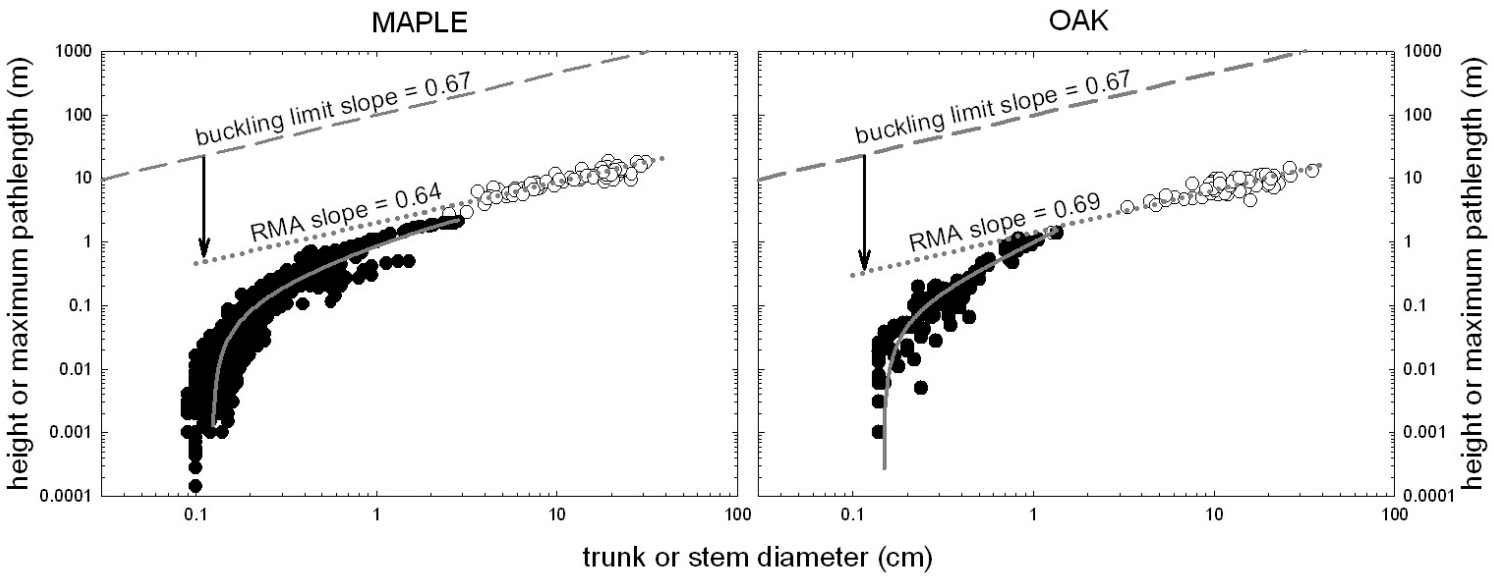

Figure 1.2. Log-log comparison of trunk (D) or stem diameter (D_s, cm) and height (H) or maximum path length (cm) in oak and maple. Open symbols are D and H data from individual trees of the same size range used to determine the sapflow scaling. Dotted lines are RMA regressions with slopes not different from the 2/3 value required for a constant safety factor (vertical arrows) from gravitational buckling (dashed line). Solid symbols are D_s vs. pathlength data within a single tree of each species with a curve fitted to illustrate the trend.

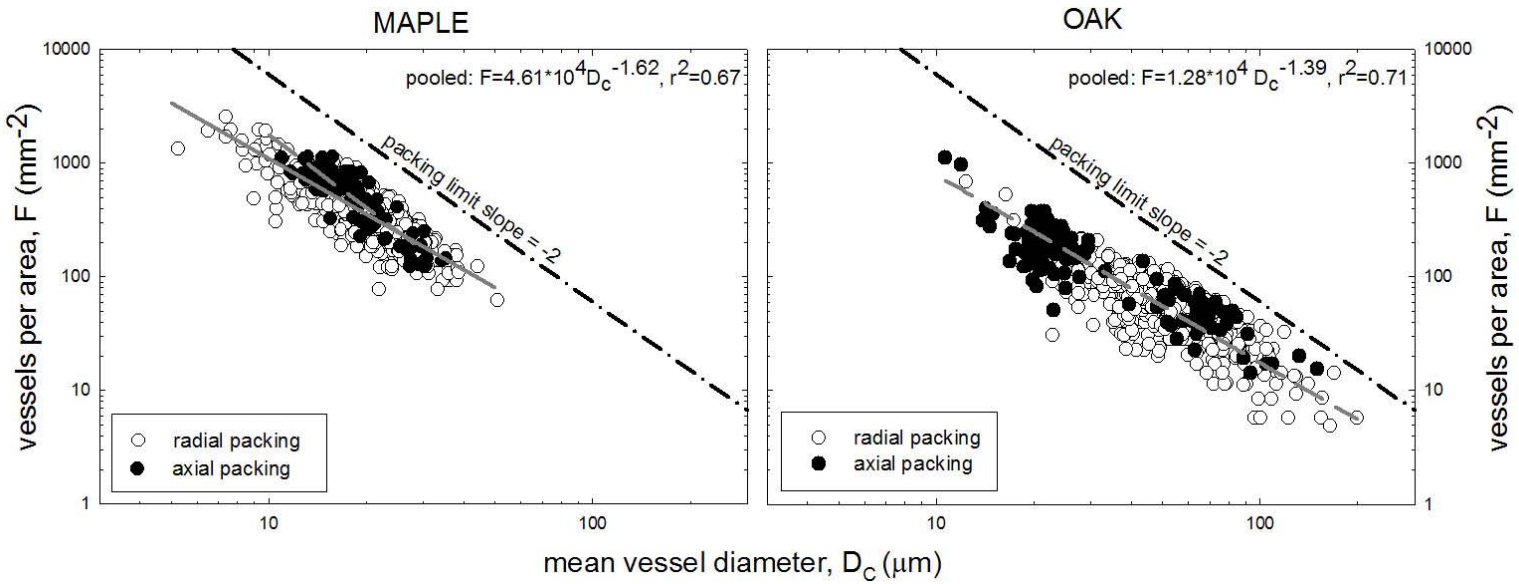

Figure 1.3. Log-log comparison of mean area-weighted vessel diameter (μm) and vessels per area (mm^{-2}). Open symbols represent radial data across all rings and all levels, while closed symbols represent axial data from the current year's growth ring at all levels. The maximum possible vessel density for a given diameter is shown as the dash-dotted packing limit. In maple (left), the axial regression (solid line) was significantly different from the radial one (dashed). In oak, axial and radial regressions were not different. The pooled regression was used as the model input for both species.

each species (Table 1.2). Interspecific comparison of pooled packing functions showed that maple and oak have species-specific packing function exponents. The less negative exponent in oak (-1.40 vs. -1.62 in maple) means that the number of vessels increases less dramatically from trunk to twig as vessels become narrower than in maple. The dot-dashed line in Figure 1.3 represents the packing limit, or the geometric limit of vessel density (F) given vessel diameter (maximum $F = 1/D_c^2$; square packing). Both species' packing functions (dashed and solid lines) are below the packing limit representing allocation of wood space to other nonconducting tissues (e.g., fibers, rays, axial parenchyma). The mean lumen area to wood area ratio for maple was 0.15 ± 0.005 and 0.15 ± 0.002 for oak.

The taper function exponent and intercepts in maple were not different between axial and radial data (Fig. 1.4). In oak, the axial intercept was different from the radial (Fig. 1.4). Again, because the model accepts only a single taper function per species, we used the pooled function as model input (Table 1.2). The taper functions were species-specific (Table 1.2). The significantly greater exponent in oak (0.39) than maple (0.15) reflects the greater vessel diameters in oak trunks (62 ± 2.9 μm) vs. maple trunks (24 ± 0.9 μm) for similar twig vessel size in both species. The greater vessel diameters and steeper taper exponent trends were expected for ring-porous oak versus smaller vessels and a shallower taper exponent in diffuse-porous maple.

Leaf-to-twig hydraulic conductance ratio (K_{leaf}/K_{twig}). Maple K_{leaf}/K_{twig} averaged 0.38 ± 0.038 (n = 5), and oak averaged 0.27 ± 0.065 (n = 4). We

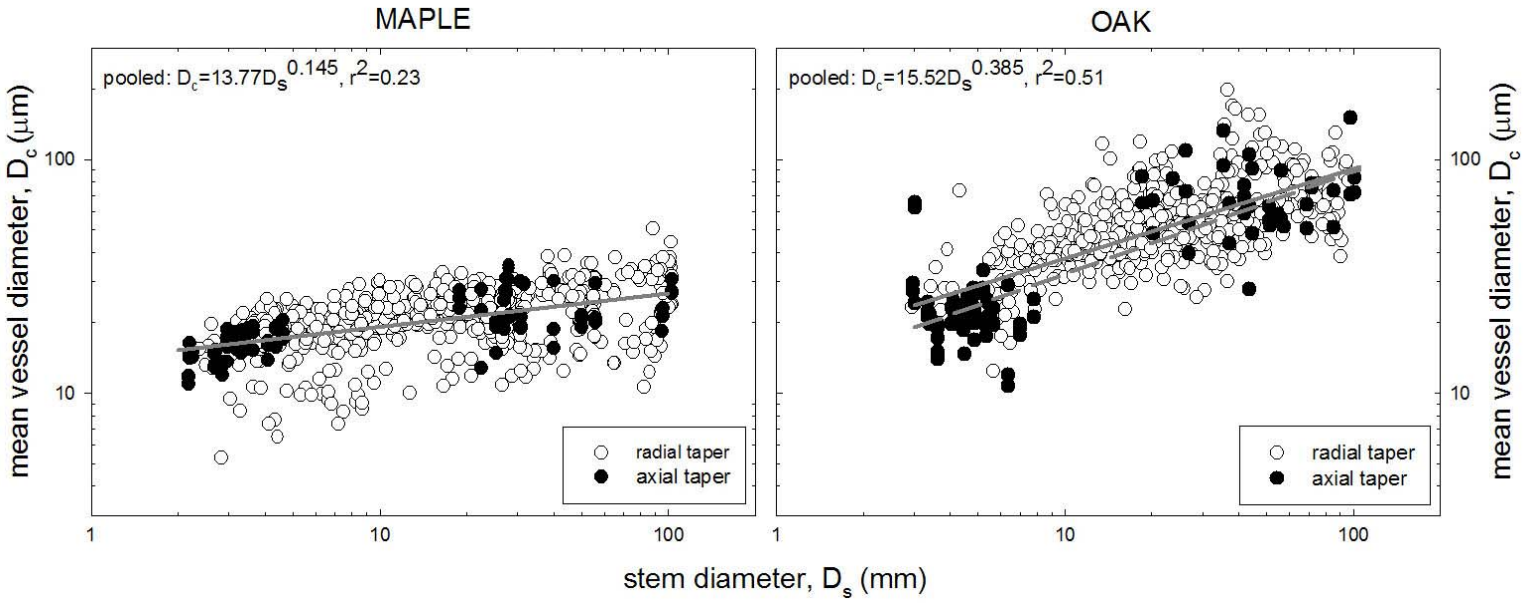

Figure 1.4. Log-log comparison of stem diameter, D_s (mm) and mean vessel diameter, D_c (μm) in oak and maple. Open symbols represent radial data across all rings and all levels, while closed symbols represent axial data from the current year's growth ring at all levels. In maple (left), axial and radial regressions were not different. In oak (right), the axial regression (solid line) was different from the radial (dashed line). The pooled regression was used as the model input for both species.

excluded an outlier in oak which had an exceptionally high ratio compared to the others (3.9 vs. 0.27). The outlier was caused by an extremely high K_{leaf} (rather than a low K_{twig}), consistent with observed petiole breakage that probably occurred during insertion of the twig into the vacuum canister.

Tree-to-shoot conductance ratio (K/K_{shoot}) and mid-day soil-canopy pressure difference (ΔP). The $\Delta P_{shoot}/\Delta P$ was independent of tree size for both species, and was used as an estimate of K/K_{shoot} for the model (Table 1.2). Maple's $\Delta P_{shoot}/\Delta P$ was 0.57 $\pm$ 0.07, meaning approximately 57% of tree hydraulic resistance was in the shoot. Oak had a much higher ratio of 0.84 $\pm$ 0.03 meaning that about 83% of the tree flow resistance was in the shoot system. The whole-tree ΔP was found to be independent of tree height as assumed by the model. The ΔP was also not different between species (maple =1.29 $\pm$ 0.03 MPa, oak = 1.32 $\pm$ 0.04 MPa; Table 1.2).

Model predictions for scaling of hydraulic conductance (K), tree water transport (Q), and growth rate with tree size

The numerical model predicts that tree conductance (K) and mid-day sapflow rate (Q) is two to three times greater in maple than oak across the experimental range (Fig. 1.5). In terms of scaling exponents, tree conductance scaling with diameter ($K \propto D^{q'}$) yields an exponent q'=1.53 (95% confidence interval: 1.44-1.71) for maple and q′=1.69 (1.59-1.78) for oak (see Table 1.3 for summary of exponents and values). Because of gravitational effects, the corresponding exponents for water transport ($Q \propto D^{q}$) are slightly less: q =1.48 (1.38-1.65) in maple and q =1.65 (1.56-1.74) in oak (Fig. 1.5). Gravitational

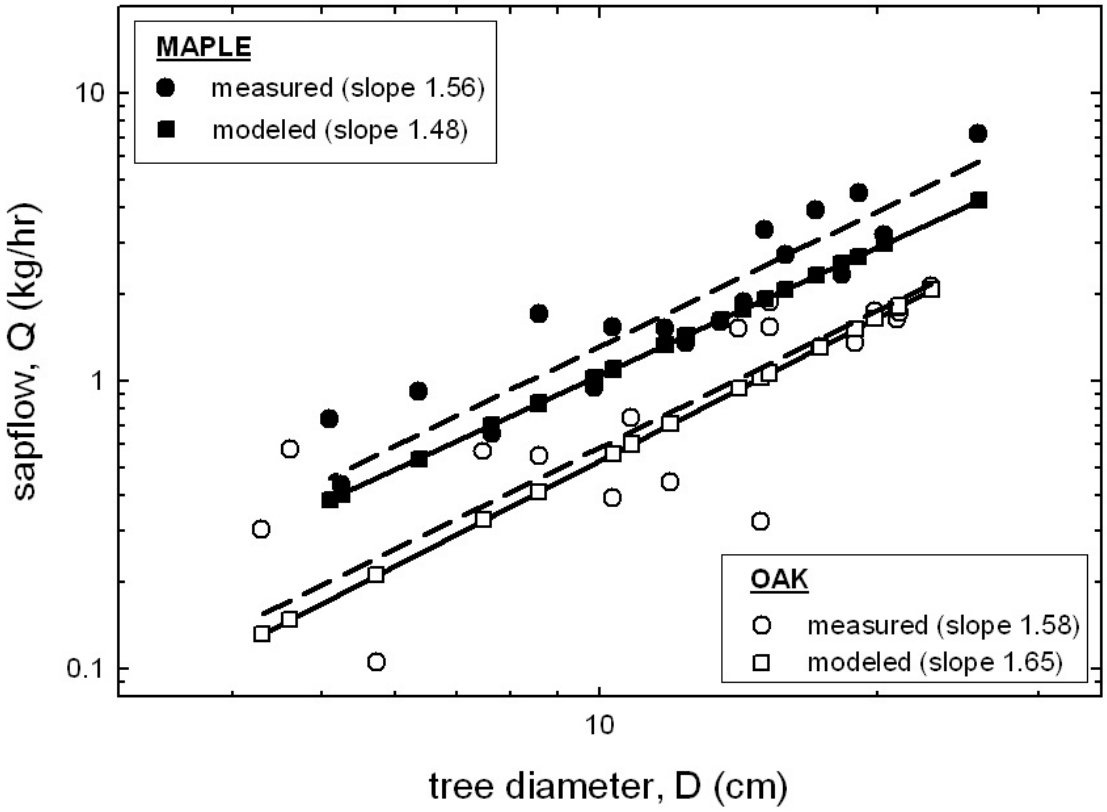

Figure 1.5. Log-log comparison of the model predictions of whole-tree water use (Q; squares) and measured tree Q (circles) versus tree diameter for maple (closed symbols) and oak (open symbols). Maple had less variability in sapflow scaling (r^2=0.85) than oak (r^2=0.59).

effects resulted in slightly allometric scaling of $Q \propto K^{0.96}$ in maple and $Q \propto K^{0.98}$ for the shorter height range of oak.

For the experimental size range, the model predicted $M \propto D^{c=0.371}$ in maple and c=0.369 in oak. Both were slightly below c=3/8=0.375 which is asymptotically approached in increasingly larger modeled trees (Sperry et al. in review). Using these c and q values, biomass growth in maple was predicted to scale with shoot mass to the cq=0.55 (0.51-0.61) power ($Q \propto B \propto M^{0.55}$), while in oak the exponent was 0.61 (0.57-0.64) power ($Q \propto B \propto M^{0.61}$). Both scaling exponents excluded the Kleiber rule value of 0.75.

Table 1.3. Modeled and measured allometric scaling exponents. Most modeled exponents were essentially without error except for q and q′ where uncertainty was captured by bootstrapping. Bootstrapping was also used to determine uncertainty for the measured c·q product. 95% confidence intervals shown.

scaling relationship	Savage model	MAPLE		OAK	
		numeric model	measured	numeric model	measured
$H \propto D^{d}$	0.67	**0.67**	**0.64** (0.57-0.71)	**0.67**	**0.69** (0.59-0.80)
$K \propto D^{q'}$	1.85	**1.53** (1.44-1.71)	**1.53** (1.20-1.87)	**1.69** (1.59-1.78)	**1.48** (0.98-1.98)
$K \propto Q$	1	**0.96**	**0.98** (0.91-1.06)	**0.98**	**0.93** (0.86-1.01)
$Q \propto D^{q}$	1.85	**1.48** (1.38-1.65)	**1.56** (1.24-1.88)	**1.65** (1.56-1.74)	**1.58** (1.05-2.12)
$D \propto M^{c}$	0.375	**0.371**	**0.39** (0.375-0.395)	**0.369**	**0.38** (0.367-0.399)
$Q \propto B \propto M^{cq}$	0.69	**0.55** (0.51-0.61)	**0.61** (0.48-0.73)	**0.61** (0.57-0.64)	**0.63** (0.41-0.83)
$B \propto M^{x}$	--	--	**0.61** (0.58-0.64)	--	**0.66** (0.61-0.71)
$B \propto Q$	1	**1**	**1.02** (0.66-1.38)	**1**	**1.13** (0.66-1.60)

Measured scaling relationships

Scaling of Q and K with D: empirical "q" exponents. The model was generally successful in predicting the observed scaling of Q and K with D, both in terms of absolute values as well as scaling exponents (Fig. 1.5 & 1.6). Predicted Q averaged 0.81 ± 0.05 times the measured Q for maple and 1.07 ± 0.16 in oak (Fig. 1.5). A "t" test indicated maple modeled vs. measured Q was significantly different while oak was not. Measured K was also directly proportional to modeled K (Fig. 1.6). Maple had 2-fold greater mid-day sapflow rate (Q) and 3-fold greater tree hydraulic conductance (K) than oak, consistent with the 2- to 3-fold difference predicted by the model.

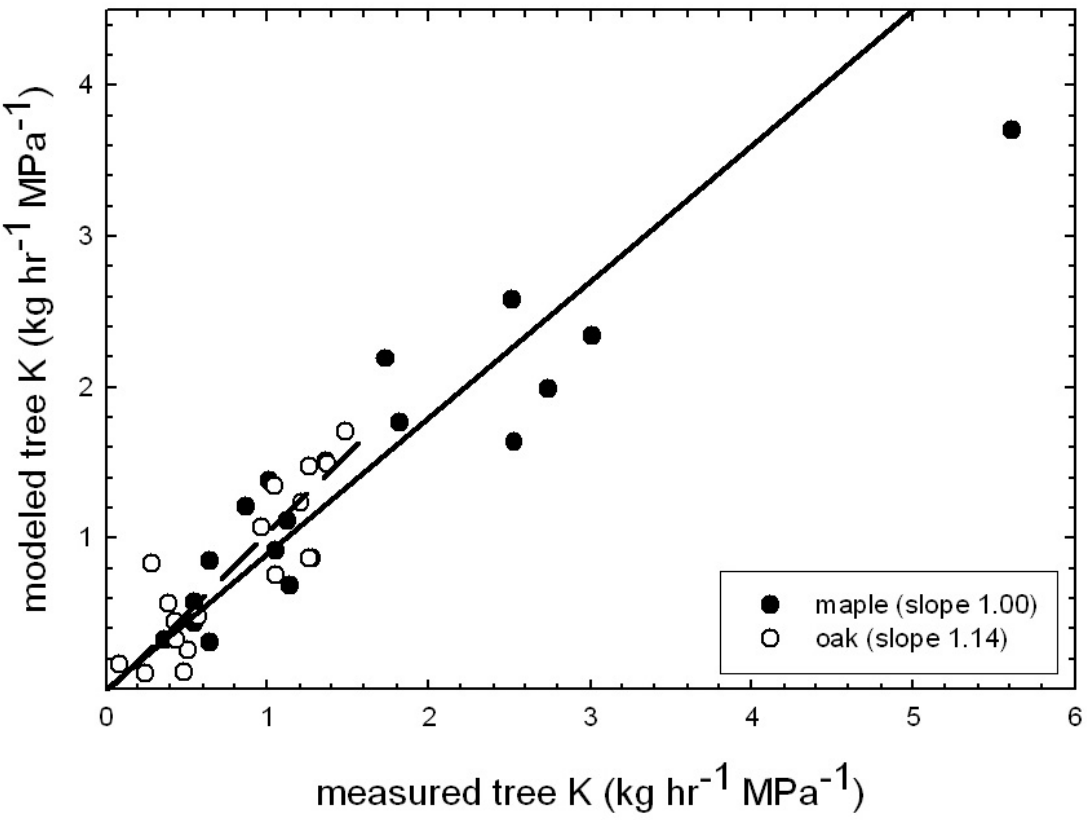

Figure 1.6. Log-log comparison of the modeled whole-tree conductance (K; kg hr^{-1} MPa^{-1}) and the measured tree K. Intercepts were not different from zero, nor were slopes different from 1, indicating successful prediction by the model.

In terms of scaling exponents, the model also did well in predicting the Q by D^q scaling (Fig. 1.5). Empirical exponent q (RMA regression) was 1.56 (95% confidence interval; 1.24-1.88) in maple (model q=1.48; 1.38-1.65) and 1.58 (1.05-2.12) in oak (model q=1.65; 1.56-1.74). The empirical q exponent was not different between species. The empirical K by $D^{q'}$ exponent of 1.53 (1.20-1.67) was identical to the model prediction in maple (1.53; 1.44-1.71). In oak, the empirical q′ of 1.48 (0.98-1.98) was less than the model estimate and below its confidence interval (1.65;1.59-1.78). Measurements supported slightly allometric scaling between $K \propto Q^{0.98}$ (0.91-1.06) in maple and $K \propto Q^{0.93}$ (0.86-1.01) in oak as predicted by the model.

Scaling of shoot mass (M) with tree size (D: empirical "c" exponents). Height and diameter data (Fig. 1.2, open symbols) was used in conjunction with wood density (ρ) measurements to estimate D by M^c scaling for trees of the size range used for sapflow measurements. Wood densities were the same in both species (oak ρ=0.64 $\pm$ 0.014 g/cm^3, maple ρ= 0.64 $\pm$ 0.009 g/cm^3). An intraspecific comparison showed that c was significantly different (maple c=0.39; 0.375-0.394, oak c=0.38; 0.367-0.399). Maple's c exponent was significantly different from the model prediction (0.371), while oak c was not different (0.369; Table 1.3). In our experimental trees, maple reached greater diameters, heights, and greater aboveground mass (233 kg) than oak (217 kg).

Shoot biomass growth rate (B) scaling with shoot mass (M); empirical "x" exponent. Maple growth rings varied much more year to year and between trees than oak (data not shown). Oak had a higher mean scaling exponent (B $\propto$

$M^{x=0.66}$; 0.61-0.71) than maple ($B \propto M^{x=0.61}$; 0.58-0.64) although they are not significantly different from each other (Fig. 1.7).

Comparison of scaling estimates for growth rate (B) with shoot mass (M). Figure 1.7 summarizes the three independent estimates for B by M scaling: 1) the model prediction from model c·q exponents, 2) the empirical prediction from empirical c·q exponents (an estimate of water transport and tree size $Q \propto B \propto M^{cq}$), and 3) the direct empirical prediction based on empirical B by M^x scaling from the tree core data.

All three estimates were similar within and between species as indicated by considerably overlapping distributions (Fig. 1.7). Means ranged from 0.55 to 0.66 (average 0.61 $\pm$ 0.039), all below the 0.75 value from Kleiber's rule. The model c·q mean differed by only 9.8% (maple) and 3.2% (oak) from the empirical c·q estimate, supporting the ability of the model to capture the scaling of mass and water transport with tree size ($Q \propto B \propto M^{cq}$). As expected, the modeled distributions were much narrower than the measured distributions in both species (Fig. 1.7).

The empirical c·q estimate ($Q \propto B \propto M^{cq}$) deviated by only 0% (maple) and 4.5% (oak) from the direct estimate from tree core data ($B \propto M^x$). Because both parameters were measured (c·q and x from cores), their distributions were similarly broad (Fig. 1.7), and overlapped considerably by 93% in maple and 74% in oak. Log likelihood values were also quite similar being 23.9 (x) vs. 23.3 (c·q) in maple and 19.8 (x) vs. 14.8 (c·q) in oak. The agreement of measured c·q and

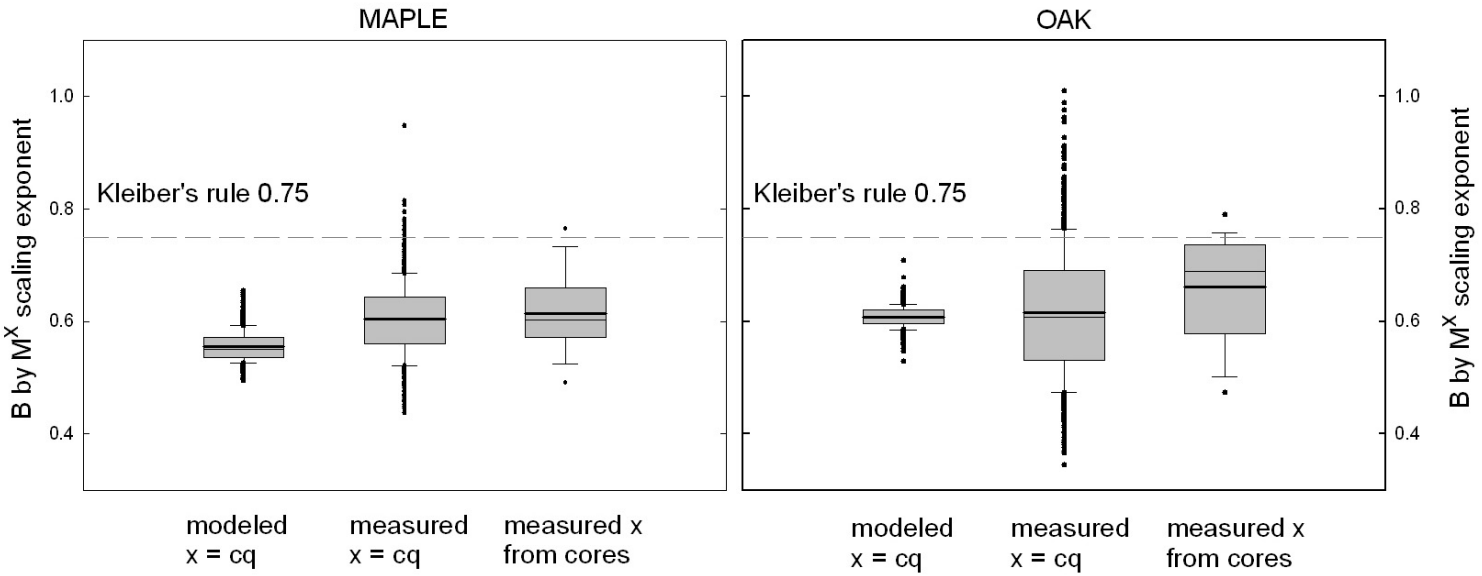

Figure 1.7. Box and whisker plots comparing three estimates of the scaling exponent "x" between shoot biomass growth rate (B) and tree shoot mass (M). The model estimates (left) are x=c·q from modeled values of c and q exponents. The measured x=c·q are from measured estimates of c and q exponents (center). Both c·q distributions were bootstrapped (n=1000). Direct measures of annual growth rates are measured x from cores (right) The measured x distribution in both cases was obtained from tree-specific scaling of B and M (n=18 per species). The heavy solid line within each box is the mean, the lighter line the median, the box the middle two quartiles (25-75 percentiles), and the bars the 10^{th} and 90^{th} percentile range. Outliers are shown by symbols. The Kleiber rule exponent of 0.75 is shown (dashed line).

the direct estimate of x validates the model assumption that $B \propto Q^1$, particularly in maple.

The isometry of B and Q was further supported by direct comparison of estimated shoot biomass growth rate from the same year (2009) that the sapflow was taken. A log-transformed linear regression (RMA) was consistent with isometry in both species (Fig. 1.8; $B \propto Q^{1.02}$ 0.66-1.38 in maple, $B \propto Q^{1.13}$ 0.66-1.60 in oak). Maple gained less shoot mass on a yearly basis per average mid-day water consumption (1.64 $\pm$ 0.21, vs. oak 0.40 $\pm$ 0.09 hour/year respectively). Although these rates are expressed over widely different time frames, it suggests that maple is less efficient at exchanging water for biomass growth than oak.

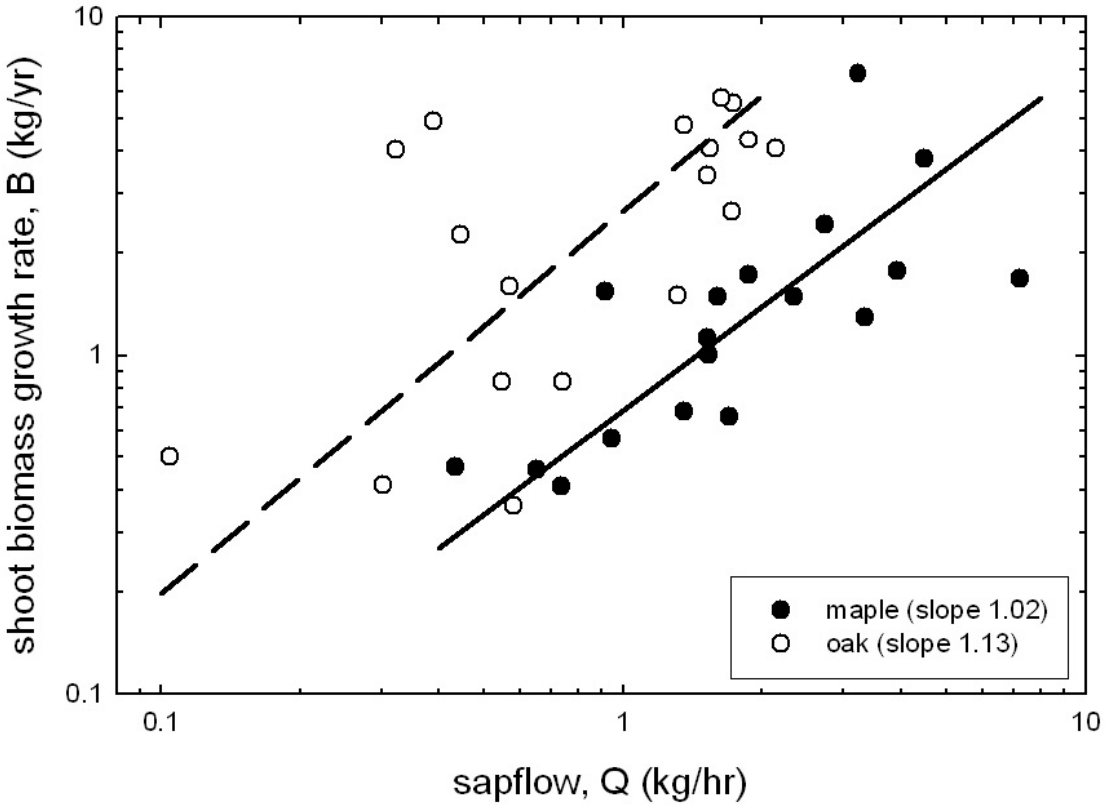

Figure 1.8. Log-log comparison of shoot biomass growth (kg/yr) and sapflow (kg/hr) using estimated biomass growth during the 2009 growing season. Maple had less variability in its B to Q scaling (r^2=0.56) than oak (r^2=0.38).

Discussion

Given its many assumptions and relatively limited inputs (Table 1.2), the species'-specific model was remarkably successful at predicting not only the hydraulic and metabolic scaling (Table 1.3, Fig. 1.7), but also the absolute values of whole-tree water use and hydraulic conductance (Figs. 1.5 & 1.6). The intent of its predecessor models, WBE and Savage, was to predict scaling exponents rather than absolute or relative interspecific values of water transport, and indeed, the Savage et al. model is successful in this regard. The 95% confidence intervals for all measurements in Table 1.3 include the predictions of the Savage model. This match is impressive considering the Savage model requires no measured inputs and does not account for species-specific differences. This suggests that the Savage model provides an extremely useful baseline for cases where the measured inputs for the numerical model are not available. Incorporation of functional group (e.g., ring-porous, diffuse-porous, and conifers) specific packing and taper functions could lead to increased scaling prediction accuracy depending on tree type.

Nevertheless, the greater realism of the numeric model improves not only the scaling estimates as intended, but also brings realistic predictions of actual water use within reach. The model is robust despite the very different anatomies of ring-porous and diffuse-porous species. The results represent the most rigorous test to date of the basic WBE concept that growth rate scales isometrically with vascular supply capacity ($B \propto Q^1$). Both model and data support the Savage model in rejecting Kleiber's rule for intraspecific scaling. Both

oak and maple show similar scaling of growth rate with mass, with various estimates of the $B \propto M^x$ exponent averaging $x = 0.61 \pm 0.039$ across species (Fig. 1.7; Table 1.3).

It is easiest to discuss the numeric model's performance in order of the logical progression from the diameter and mass relationship ($D \propto M^c$), to the whole-tree hydraulic conductance by diameter scaling ($K \propto D^{q'}$) and whole-tree water use by diameter scaling ($Q \propto D^q$), and finally to the growth rate and mass scaling ($Q \propto B \propto M^{cq}$) prediction. Seemingly the most robust relationship was the prediction of exponent c ($D \propto M^c$), where the model was within 3-5% of measured estimates (Table 1.3). This was consistent with the validation of DaVinci's rule (Fig. 1.1) and the convergence to elastic similarity (Fig. 1.2). These concepts are well established and are generally supported across a range of species (McMahon 1973, Niklas 1994, King 1986).

The numeric model was more variable in its prediction of K by $D^{q'}$ scaling, ranging from 0% deviation in q' prediction for maple to 12.4% deviation in oak. The over-prediction in oak (1.69 vs. measured 1.48) may simply reflect the greater variability in empirical Q by D data from which the K by D scaling was derived (Fig. 1.5). The model was reasonably accurate in predicting absolute K, with model values scaling in direct proportion to measurements (Fig. 1.6). Contributing to this accuracy was the incorporation of three empirical "correction factors" that account for 1) conduit end-walls (K_x/K_{HP}; Table 1.2), 2) leaf conductance (K_{leaf}/K_{twig}; Table 1.2), and 3) root conductance (K/K_{shoot}; Table 1.2). Nevertheless, sources of uncertainty remain. Xylem cavitation (conduit failure) is

not accounted for, nor is the presence of extra-vascular resistances in roots and leaves, both of which would tend to make the model over-estimate the measured tree hydraulic conductance. In addition, conduit diameter variation was represented by the area-weighted average rather than a conductance-weighted average, which would tend to under-estimate the true xylem conductance.

Another potentially important factor that is not included in the current model is the effect of deviations from the assumption of strictly self-similar and symmetric branching structure. Real trees generally show asymmetric branching with varying degrees of apical dominance. The effect of branching structure on K by D scaling is complex, and based on preliminary analysis is likely to influence absolute values more than scaling exponents (D. Smith and J. Sperry, unpubl. observations). Incorporating more realism in the branch network is an important next step towards model improvement.

Model predictions of Q by D^q scaling were within 5.1% (maple) and 4.2% (oak) of measured values. Based as they were on predictions of K by $D^{q'}$ and $\Delta P'$ ($Q = K \Delta P'$), it is not surprising that they were similarly accurate. Contributing to the accuracy was the validity of the model assumption that ΔP ($= \Delta P' + \rho g H$) was invariant with tree size. Model predictions of absolute Q deviated by 29% (maple) and 7% (oak) from measured water use. Although not as accurate as the scaling predictions, this degree of agreement with absolute values was surprising given the simplicity of the model. In addition, the model was quite accurate in predicting relative water consumption between maple and oak.

At the ecophysiological scale, predicting interspecific differences in water consumption provides insights into competitive interactions. Interestingly, although maple used more water than oak, it did not translate into greater growth rates (which were similar between species), because maple was less efficient in converting water use to shoot biomass than oak (Fig. 1.8). A simple explanation of this would be greater allocation of carbon to the high turnover costs associated with surface roots in maple. Fine root networks in shallow roots are also consistent with greater relative root system conductance (Table 1.2). At the stand and ecosystem scale, the accuracy of the model raises the possibility of employing it in ecohydrological applications, where stand or watershed level estimates of water use are required (Novick et al. 2009). Accurate predictions of water use per tree size can lead to reasonable estimates of water use at the stand level and up to ecosystems if the relative distribution of species and their diameters are known.

Important caveats to the model prediction of Q are circumstances under which ΔP may not be constant. The height range of our trees, though maximal for the habitat and region, was small (Fig. 1.2). Some tree species, particularly taller ones, have been reported to increase ΔP with height (Phillips et al. 2002, Barnard and Ryan 2003). An increase in ΔP with height would cause the model to under-predict Q and q. Soil drought is another important circumstance that could alter ΔP, reducing it for a given height for isohydric species that maintain relatively constant canopy xylem pressure. Even in anisohydric species, which tend to drop canopy xylem pressure with soil drought and preserve ΔP, a

concomitant increase in xylem cavitation would alter the model predictions. These soil drying effects would cause the model to over-predict Q scaling. These ΔP and cavitation issues could be incorporated in to future revisions of the model, but will come at the cost of increased complexity.

The combination of $D \propto M^c$ and $Q \propto D^q$ predicts that $Q \propto M^{cq}$. Given the success of the "c" and "q" estimation, the similar accuracy of the c·q estimate was expected. The modeled value of cq was within 9.8% (maple) and 3.2% (oak) of measured values (Table 1.3).

Perhaps the most critical and fundamental assumption of the model is that growth rate will scale isometrically with water transport: $B \propto Q^1$. This is the rationale for predicting Q from vascular structure in the first place, so that metabolic scaling can be predicted from the chain of proportionalities: $Q \propto B \propto M^{cq}$. Two linked lines of evidence supported the $B \propto Q^1$ assumption. The first is that measured $Q \propto M^{cq}$ scaling agreed extremely well with direct measurements of $B \propto M^x$ scaling: the c·q exponent was within 0% (maple) and 4.5% (oak) of the "x" estimated from tree core data (Fig. 1.7). This could only happen if B was nearly isometric with Q. The second line of evidence is that plotting estimates of annual B against Q yielded scaling exponents of 1.02 (maple) and 1.13 (oak): within 2-13% of isometry.

The approximate isometry of growth rate and water use is a surprisingly simple outcome of a very complex chain of events. Transpiration presumably must be isometric with net CO_2 uptake, which requires CO_2 uptake to be diffusion-limited rather than reaction limited, which implies coordination between

resource allocation (primarily nitrogen) to photosynthetic pigments and enzymes and the supply of water to the leaf. Net assimilation (A) is distributed to net biomass growth in the shoot (B) and the root (not measured), as well as to respiration, reproduction, volatile compounds, root exudation, and loss of parts. For B to scale isometrically with A and Q, either all of these allocations must also be isometric, or there are compensatory effects which preserve the isometry of B. Nevertheless, the assumption of $B \propto Q^1$ was supported in our case study, and whether it is generally confirmed awaits further analysis. Extending the model to include carbon allocation would allow it to predict relative B values as well as Q, making it even more of a useful tool.

Kleiber's rule, at least for intraspecific scaling, was not supported by the model or the measurements. Other studies also support scaling exponents in the 0.50 – 0.66 range for intraspecific data (Mencuccini 2003, Sperry et al. 2008). Simulations using the numerical model parameterized for several functional tree types suggest that the highest scaling exponents would be achieved by tropical trees and reach an upper limit of around 0.72. The lowest exponents would potentially be achieved by ring-porous trees, dropping below 0.50 (Sperry et al. in review). This functional type analysis also suggests that not only do tree species not follow Kleiber's rule, they do not follow any other single rule, with variation in scaling exponents reflecting multiple optima in safety vs. efficiency trade-offs across functional types and habitats.

In conclusion, our results strongly support the basic assumption underlying metabolic scaling theory, that growth rate is proportional to vascular

supply ($B \propto Q$). The greater realism of the numerical model relative to its WBE and Savage predecessors allows accurate predictions of species' and size-specific scaling exponents. Kleiber's rule for intraspecific scaling of trees can be rejected (when $B \propto Q$). In addition, the model can accurately predict interspecific differences in plant hydraulic conductance and water consumption, as well as make reasonable estimates of absolute values of water use, from relatively few parameters. The success of the model argues for extending it to account for branching architecture and carbon allocation. The potential utility of the model is diverse, expanding beyond allometric studies to analysis of ecophysiology and ecological interactions, ecohydrology, and ecosystem processes.

Acknowledgements

We thank Henry Grover and Andy Crawl for field assistance, Susan Bush and Kevin Hultine for technical support of sapflow measurements and calibrations, and Margerieth Christman for help in the laboratory. Fred Adler of the University of Utah helped tremendously with data analysis and interpretation. Funding came from NSF-IBN-0743148 to JSS and NSF-ATB-0742800 to BJE.

Literature Cited

Baas, P. 1986. Ecological patterns of xylem anatomy. Pages 327-351 *in* T. J. Givnish, editor. On the Economy of Plant Form and Function. Cambridge University Press, Cambridge.

Barnard, H. R. and M. G. Ryan. 2003. A test of the hydraulic limitation hypothesis in fast-growing *Eucalyptus saligna*. Plant Cell and Environment **26**:1235-1245.

Bush, S. E., K. R. Hultine, J. S. Sperry, and J. R. Ehleringer. 2010. Calibration of thermal dissipation sapflow probes for ring- and diffuse-porous trees. Tree Physiology **30**:1545-1554.

Calkin, H. W., A. C. Gibson, and P. S. Nobel. 1986. Biophysical model of xylem conductance in tracheids of the fern *Pteris vittata*. Journal of Experimental Botany **37**:1054-1064.

Crow, T. R. 1978. Common regressions to estimate tree biomass in tropical stands. Forest Science **24**:110-114.

Edwards, A. W. F. 1992. Likelihood. John Hopkins University Press, London.

Ehleringer, J. R., L. A. Arnow, T. Arnow, I. B. McNulty, and N. C. Negus. 1992. Red Butte Canyon Research Natural Area: history, flora, geology, climate, and ecology. Great Basin Naturalist **52**:95-121.

Enquist, B. J. and K. J. Niklas. 2001. Invariant scaling relations across tree-dominated communities. Nature **410**:655-660.

Enquist, B. J., B. H. Tiffney, and K. J. Niklas. 2007. Metabolic scaling and the evolutionary dynamics of plant size, form, and diversity: Toward a synthesis of ecology, evolution, and paleontology. International Journal of Plant Sciences **168**:729-749.

Enquist, B. J., G. B. West, E. L. Charnov, and J. H. Brown. 1999. Allometric scaling of production and life-history variation in vascular plants. Nature **401**:907-911.

Gibson, A. C., H. W. Calkin, and P. S. Nobel. 1984. Xylem anatomy, water flow, and hydraulic conductance in the fern *Cyrtomium falcatum*. American Journal of Botany **71**:564-574.

Granier, A. 1985. Une nouvelle methode pour la mesure du flux de seve brute dans le tronc des arbes. Annales des Sciences Forestieres **42**:193-200.

Greenhill, A. G. 1881. Determination of the greatest height consistent with stability that a vertical pole or mast can be made, and the greatest height to which a tree of given proportions can grow. Proceedings of the Cambridge Philosophical Society.

Hacke, U. G., J. S. Sperry, J. K. Wheeler, and L. Castro. 2006. Scaling of angiosperm xylem structure with safety and efficiency. Tree Physiology **26**:689-701.

Hubbard, R. M., V. Stiller, M. G. Ryan, and J. S. Sperry. 2001. Stomatal conductance and photosynthesis vary linearly with plant hydraulic conductance in ponderosa pine. Plant Cell and Environment **24**:113-121.

King, D. A. 1986. Tree form, height growth, and susceptibility to wind damage in *Acer saccharum*. Ecology **67**:980-990.

Kleiber, M. 1932. Body size and metabolism. Hilgardia **6**:315-353.

Kolb, K. J. and S. D. Davis. 1994. Drought tolerance and xylem embolism in co-occurring species of coastal sage and chaparral. Ecology **75**:648-659.

Makarieva, A. M., V. G. Gorshkov, B. L. Li, S. L. Chown, P. B. Reich, and V. M. Gavrilov. 2008. Mean mass-specific metabolic rates are strikingly similar across life's major domains: Evidence for life's metabolic optimum. Proceedings of the National Academy of Sciences of the United States of America **105**:16994-16999.

McCulloh, K. A., J. S. Sperry, and F. R. Adler. 2003. Do plants obey Murray's law? Nature **421**:939-942.

McMahon, T. A. 1973. Size and shape in biology. Science **179**:1201-1204.

Mencuccini, M. 2003. The ecological significance of long-distance water transport: short-term regulation, long-term acclimation and the hydraulic costs of stature across plant life forms. Plant Cell and Environment **26**:163-182.

Niklas, K. J. 1994. The allometry of safety-factors for plant height. American Journal of Botany **81**:345-351.

Niklas, K. J. and B. J. Enquist. 2001. Invariant scaling relationships for interspecific plant biomass production rates and body size. Proceedings of the National Academy of Sciences of the United States of America **98**:2922-2927.

Niklas, K. J. and B. J. Enquist. 2003. An allometric model for seed plant reproduction. Evolutionary Ecology Research **5**:79-88.

Novick, K., R. Oren, P. Stoy, J. Y. Juang, M. Siqueira, and G. Katul. 2009. The relationship between reference canopy conductance and simplified hydraulic architecture. Advances in Water Resources **32**:809-819.

Phillips, N., B. J. Bond, N. G. McDowell, and M. G. Ryan. 2002. Canopy and hydraulic conductance in young, mature and old Douglas-fir trees. Tree Physiology **22**:205-211.

Richter, J. P. 1970. The notebooks of Leonardo da Vinci (1452-1519), compiled and edited from the original manuscripts. Dover, New York.

Reich, P. B., M. G. Tjoelker, J. L. Machado, and J. Oleksyn. 2006. Universal scaling of respiratory metabolism, size and nitrogen in plants. Nature **439**:457-461.

Ryan, M. G., N. Phillips, and B. J. Bond. 2006. The hydraulic limitation hypothesis revisited. Plant Cell and Environment **29**:367-381.

Savage, V. M., L. P. Bentley, B. J. Enquist, J. S. Sperry, D. D. Smith, P. B. Reich, and E. I. von Allmen. 2010. Hydraulic trade-offs and space filling enable better predictions of vascular structure and function in plants. Proceedings of the National Academy of Sciences of the United States of America **107**:22722-22727.

Sperry, J. S., F. C. Meinzer, and K. A. McCulloh. 2008. Safety and efficiency conflicts in hydraulic architecture: scaling from tissues to trees. Plant Cell and Environment **31**:632-645.

Warton, D. I., I. J. Wright, D. S. Falster, and M. Westoby. 2006. Bivariate line-fitting methods for allometry. Biological Reviews **81**:259-291.

West, G. B., J. H. Brown, and B. J. Enquist. 1997. A general model for the origin of allometric scaling laws in biology. Science **276**:122-126.

West, G. B., B. J. Enquist, and J. H. Brown. 2009. A general quantitative theory of forest structure and dynamics. Proceedings of the National Academy of Sciences of the United States of America **106**:7040-7045.

Wheeler, J. K., J. S. Sperry, U. G. Hacke, and N. Hoang. 2005. Inter-vessel pitting and cavitation in woody Rosaceae and other vesselled plants: a basis for a safety vs. efficiency trade-off in xylem transport. Plant Cell and Environment **28**:800-812.

Wilson, K. B., P. J. Hanson, P. J. Mulholland, D. D. Baldocchi, and S. D. Wullschleger. 2001. A comparison of methods for determining forest evapotranspiration and its components: sap-flow, soil water budget, eddy covariance and catchment water balance. Agricultural and Forest Meteorology **106**:153-168.

Zimmermann, M. H. 1983. Xylem structure and the ascent of sap. Springer, Berlin, Heidelberg, New York.

CHAPTER 2

COMPARATIVE WATER USE, HYDRAULICS, AND GROWTH RATES IN COEXISTING RING-POROUS (QUERCUS GAMBELII) AND DIFFUSE-POROUS (ACER GRANDIDENTATUM) SPECIES

Abstract

The co-dominant and functionally diverse *Quercus gambelii* (Gambel oak, ring-porous) and *Acer grandidentatum* (bigtooth maple, diffuse-porous) are able coexist due to different hydraulic architecture and different water use niches that result in similar growth rates. We address two main questions in this study: how do rates of water transport vary between species, and how does water use translate into growth rates. To answer these questions we measured sapflow and hydraulic conductance, leaf area, and growth rates in each species. Ring-porous Gambel oak has much lower peak and seasonal sapflow and lower whole-tree conductance than diffuse-porous bigtooth maple, yet by virtue of a more efficient exchange of water for shoot growth it achieved similar shoot biomass growth rates as bigtooth maple. Gamble oak had more stable rates of water uptake, suggestive of deep-rooting while bigtooth maple appeared to be more opportunistic in its water use implying greater reliance on shallower roots.

Consequently, growth rates in bigtooth maple were much more variable on a year-to-year basis.

Introduction

In the Intermountain West of the U.S. between the low elevation grass-shrublands and the high elevation spruce-fir forests lies the mid-elevation shrub woodland with *Acer grandidentatum* (Nutt) and *Quercus gambelii* (Nutt) as co-dominant deciduous hardwoods. This habitat experiences summer droughts and vegetation cover is defined primarily by soil moisture availability. Although much is known about *Acer-Quercus* woodlands in this region qualitatively, relatively little is known about how well these sympatric species compete for water and how their water consumption relates to differences in their growth rates. Here we investigate how these co-dominant species can grow side-by-side in the same habitat yet transport water using contrasting wood anatomies (diffuse- vs. ring-porous anatomy). Our two main questions are: 1) Do the differences in wood anatomy translate to different rates of tree water transport between species? and 2) How do differences in water consumption relate to differences in growth rates?

Diffuse-porous species, such as *A. grandidentatum* (bigtooth maple hereafter), transport water using many relatively small vessels (bigtooth maple # vessels/area mean $\pm$ SE = 346 $\pm$ 31 μm^{-2} and mean vessel diameter = 24 $\pm$ 1 μm, N=94) across multiple growth rings (von Allmen et al., in prep). Temperate diffuse-porous species have vessel sizes that are small enough to tolerate freezing without much embolism or xylem failure (Davis et al. 1999, Zimmermann 1983). There is a tendency for little freezing embolism (breakage of water column

in xylem due to freeze-thaw cycles) and loss of conductivity over the winter in diffuse-porous species. Limited embolism and spring refilling mechanisms in many species (Sperry and Sullivan 1992, Hacke and Sauter 1996), enable early bud break in the spring giving diffuse-porous species a competitive advantage for acquiring available resources early in the season (Wang et al. 1992, Lechowicz 1984, Zimmermann and Brown 1971). Although tolerance to freezing embolism and early bud break are true of most temperate diffuse porous species, their vulnerability to cavitation (breakage of the water column by air filled vessels) by drought varies considerably (Sperry and Sullivan 1992). Some diffuse-porous species, such as bigtooth maple, are relatively resistant to xylem cavitation from drought stress. Taneda and Sperry (2008) found bigtooth maple maintained 50% of potential hydraulic conductance even under moderate-to-high water stress conditions (-4.79 MPa; as water stress increases, water potentials become more negative). Tolerance to water stress should enable bigtooth maple to have looser stomatal regulation and a greater portion of shallow roots, resulting in anisohydric behavior where canopy water status is affected by soil water deficit. Studies have shown bigtooth maple water potentials respond to drought and rain events, indicating shallow rooting and anisohydric water status (Taneda and Sperry 2008, Phillips and Ehleringer 1995). The overall strategy of bigtooth maple appears to be to compete for early season resources with early leaf-out, resulting in high rates of gas exchange early in the season followed by more moderate gas exchange during mid- and late-summer as water stress induces stomatal closure. The trade-off to rapidly using surface soil water is that the surface soil moisture

becomes exhausted earlier in the summer, potentially resulting in water stress, decreased water transport and earlier leaf senescence.

In contrast to diffuse-porous species, ring-porous species, such as *Q. gambelii* (Gambel oak hereafter) have fewer, much larger vessels (Gambel oak # vessels/area mean $\pm$ SE = 47 $\pm$ 3 μm^{-2} and mean vessel diameter = 62 $\pm$ 3 μm, N=69) in the earlywood and much smaller vessels in the latewood (von Allmen et al., in prep). Large earlywood vessels embolize predictably when the frozen xylem conduits thaw, resulting in near complete loss of hydraulic conductance over the winter. These earlywood conduits do not refill in the spring, and therefore, the active conducting sapwood area is limited to the current year's growth ring (Zimmermann 1983, Sperry and Sullivan 1992, Ellmore and Ewers 1986). Each spring, ring-porous species must form new earlywood vessels to provide adequate water and resource transport for buds, resulting in much later bud break (Wang et al. 1992, Lechowicz 1984, Zimmermann and Brown 1971). Bigtooth maple has finished its flower cycle and is well into leaf out before Gambel oak has begun to break bud (Phillips and Ehleringer 1995). When Gambel oak buds emerge, the leaves reach full size very quickly. It has been suggested that this mass leaf-out could be a mechanism to overwhelm leaf herbivores (Wang et al. 1992). In addition to failure from freezing embolism, a portion of the large vessels of ring-porous species are also vulnerable to xylem cavitation from soil moisture drought (Sperry and Sullivan 1992). Taneda and Sperry (2008) showed that Gambel oak experiences 50% loss in conductivity at very low water stress (-0.25 MPa) due to earlywood xylem cavitation, nearly a

10-fold difference from bigtooth maple. Although Gambel oak experiences a large decrease in conductivity at low negative pressures, water continues to flow through remaining functional earlywood vessels which are rather resistant to cavitation and do not reach 100% loss of conductivity until about -4.5 MPa (Sperry and Sullivan 1992). The latewood vessels are generally too small and few in number to contribute significantly to transpirational flow. The large vessels in Gambel oak enable maximum potential hydraulic conductance to reach much higher potential conductance than bigtooth maple. Roughly 90% of these large ring-porous vessels could cavitate and Gambel oak would still maintain the same water conducting capacity as fully functioning conductivity in bigtooth maple vessels (Hacke et al. 2006). The trade-off for having large vessels capable of highly efficient water transport appears to be the risk of vessel failure from drought stress as well as freeze-thaw events. Hence, many of the earlywood vessels appear to be nonfunctional at mid-day because they are cavitated and the hydraulic conductivity of similar-sized Gambel oak branches can actually be less than bigtooth maple branches (Taneda and Sperry 2008). Consistent with the minimization of cavitation from drought stress, Gambel oak tightly controls its stomata and invests in deep roots accessing more reliable soil moisture (Taneda and Sperry 2008, Phillips and Ehleringer 1995).

Soil moisture in this region is dependent on winter precipitation, with roughly 80% of precipitation from snow and about 20% from rain (Dobrowolski et al. 1990). Summer precipitation is unpredictable and has large variation in magnitude and soil wetting capacity. Like most plants in the Intermountain West,

both bigtooth maple and Gambel oak use the previous season's winter snowmelt via deep roots that access deep soil moisture. Studies show Gambel oak to be isohydric with reliable water status despite long durations without rain, suggesting relatively more reliance on deep roots (Taneda and Sperry 2008, Bush et al. 2008, Phillips and Ehleringer 1995). Conversely, bigtooth maple invests more in shallow roots presumably to take advantage of the shallow precipitation and early snowmelt (Taneda and Sperry 2008, Phillips and Ehleringer 1995). Stable isotope analysis showed that bigtooth maple took up water from the largest summer rain events (Phillips and Ehleringer 1995). Phillips and Ehleringer (1995) found that juvenile trees of both species rely on shallow roots and surface soil moisture from summer rains for establishment.

Both these species have low seedling establishment away from riparian corridors, likely due to severe water stress before saplings establish deep roots to access deep soil water (Taneda and Sperry 2008, Neilson and Wullstein 1983). The two species persist in drier habitats with deeper water tables only by means of asexual reproduction via root-sprouting from long-lived clones (Neilson and Wullstein 1985). Tiedeman et al. (1987) noted enlarged stem-like structure at the base of Gambel oak trunks, called lignotubers, which have a high density of adventitious buds below the soil capable of giving rise to new shoots. These same structures enable for resprouting after fires (Tiedemann et al. 1987, Engle 1983).

Although bigtooth maple and Gambel oak have vastly different vascular anatomy they have similar stature or external growth forms and co-occur in

extensive stands. We strive to better understand how the different vascular structure of these sympatric species relates to their transport capacity, water consumption, growth rates, and water-for-biomass conversion efficiency. Are these two species with contrasting vascular anatomy moving similar amounts of water and growing at similar rates in order to coexist in the same habitat? To test these questions we measured sapflow and xylem pressure measurements to characterize whole-tree hydraulics throughout a growing season, and we estimated aboveground biomass growth rates from allometric relationships and tree cores. The two species were studied across a broad size range and in mixed stands. The stands were located in a riparian woodland to minimize effects of soil moisture, thus maximizing the ability to detect interspecific differences based on vascular architecture.

Methods

Study site

Red Butte Canyon Research Natural Area (RNA) is the study site, approximately 8 km east of Salt Lake City, Utah at 40° 47′ latitude and 111° 48′ longitude with an elevation gradient of 1530 to 2510 m. Red Butte Canyon receives roughly 500 mm of rain annually at lower elevations (Ehleringer et al. 1992). Individuals of *A. grandidentatum* (bigtooth maple) and *Q. gambelii* (Gambel oak) were selected along the riparian corridor with full canopies in the sun and as part of tree stands. A riparian habitat was chosen because this is where both species exhibit the widest range in size and suffers the least soil

moisture stress, thus highlighting the differences resulting from vascular anatomy.

Climate and meteorological data

Temperature and percent relative humidity were measured (HMP35C, HMP50, CS500; Campbell Scientific, Logan, Utah) at each of three locations every 30 s and averaged and stored every 30 min in dataloggers (CR7X; Campbell Scientific, Logan, Utah) from June through September 2009. The air temperature and relative humidity were used to calculate atmospheric vapor pressure deficit (VPD). Photosynthetic active radiation (PAR) was measured with a Li-cor quantum sensor (LI-190SZ, Li-cor Biosciences, Lincoln, Nebraska) every 30 s and averaged every 30 minutes by a datalogger (CR10X; Campbell Scientific, Logan, Utah) roughly 1 km away at an existing weather station in Red Butte Canyon. Daily precipitation was measured at the same weather station using a tipping-bucket rain gauge (TE525; Campbell Scientific, Logan, Utah).

Measuring whole-tree sapflow and whole-tree conductance

Whole-tree sapflow (Q) and conductance (K) were measured across a range of tree diameters (D) in each species from Red Butte Canyon RNA (Gambel oak D: 4-23 cm, bigtooth maple D: 5-26 cm). The upper diameter range approached the maximum for this riparian forest. Three study locations (1660 m, 1680 m, 1730 m) were chosen along the riparian corridor. These sites were selected to have similar stand structure (continuous stands without isolated

individuals). At each site, 12 trees were selected with upper canopies in full sun. Across sites there was a total 18 individuals from each species.

Whole-tree water use or sapflow (Q). The rate of water transport (Q) was measured at each tree using heat dissipation sensors (Granier 1985). Paired sensors were inserted 15 cm apart (axially) on random sides of the tree trunk at breast height. Standard Granier probes (20 mm long) were used in bigtooth maples, while shorter probes (10 mm long) were used with their independent calibration for Gambel oak is due to their shallow active xylem layer. For a more detailed explanation of sapflow and calibration methodology please see methods in Ch. 1. Sapflow from sensors was measured every 30 seconds and averaged every 30 minutes using dataloggers (CR7X, Campbell Scientific, Logan, Utah) from mid-June until leaf senescence (June 15-Oct 31, 2009).

To obtain whole-tree sapflow (Q) from sensors in the field, sapwood area (A_{sw}) was measured from each experimental tree, using a 12 mm increment borer (Haglöf, Sweden). From each tree, cores were collected between sensors. To obtain more details about sapwood area methodologies please see the methods section in Ch. 1. Clearwater (1999) correction was applied to any bigtooth maple probe that exceeded the depth of sapwood. Sapflow (Q) was calculated for each tree by multiplying sapflow density and sapwood area ($Q=Q/A_{sw} * A_{sw}$). To determine daily sapflow, sapflow (per hour) was multiplied by the number of daylight hours.

Maximum sapflow (Q_{max}) under well-watered conditions should be limited only by stomatal regulation of canopy xylem pressure rather than by low light, soil

moisture, or VPD. For Q_{max} we did not use Q data from cloudy days, or from periods where predawn xylem pressures became more negative, which indicated soil drought in the rooting zone. To filter low VPD periods we plotted Q for each tree versus the corresponding day's mean VPD. All Q data below the top 10% across the VPD range were excluded. Mid-day Q_{max} was obtained from the average of the top 5 daytime values from filtered data (each a 30 minute mean). The relationship of Q_{max} and diameter gave the scaling exponent q ($Q_{max} \propto D^q$). To eliminate the effects of tree size on sapflow, we divided the mean daily sapflow from each individual tree by D^q resulting in standardized sapflow (Q_s).

Whole-tree conductance (K). Xylem pressures were measured at roughly 10 day intervals over the growing season on the sapflow trees. Pressures were measured on excised leaves (n=3 per tree) with a Scholander pressure chamber (PMS Instruments Co., Corvallis, Oregon). On a give date, up to three types of pressure measurements were made for each tree: predawn pressures from leaves near ground level ($P_{PD,}$ 0400-0600 hr, assumed to approximate soil water potential in the rooting zone), mid-day canopy pressure (P_{MD}; 1100-1400 hr), and mid-day root-crown pressure (P_{RC}; 1200-1400 hr). To measure P_{RC}, we covered all leaves on shoots attached near the root crown with foil and to allowed xylem pressures to equilibrate with the root crown pressure for 1 hour. Covered leaves were then cut and immediately measured in the pressure chamber. Because of limitations on the number of shoots available for P_{RC} measurements, we could only measure P_{RC} on a subset of measurement days.

Soil-to-leaf pressure drop (ΔP) was calculated from P_{PD}-P_{MD}. To account for tree height we subtracted the drop in pressure due to gravity ($\Delta P'$; $\Delta P' = \Delta P - \rho gH$, where P is in MPa, and H is tree height in meters, and ρg=0.009781 in MPa/m). The $\Delta P'$ is the pressure drop associated with the transpiration stream. The estimated whole-tree conductance (K) for each tree was the mid-day size-standardized Q divided by $\Delta P'$ ($K= Q_s/\Delta P'$). Thus, K values were also effectively corrected for size-dependence. Standardized whole-tree conductances were averaged over all individuals at each site from the sampling date.

Portion of hydraulic resistance in shoot. For days when P_{PD}, P_{RC}, and P_{MD} were measured on the same trees, we estimated $\Delta P_{shoot}/\Delta P$ from $(P_{RC}-P_{MD})/(P_{PD}-P_{MD})$. The $\Delta P_{shoot}/\Delta P$ ratio equates to the fraction of whole-tree hydraulic resistance that is in the shoot system.

Leaf hydraulic conductance per leaf area (K_L). Leaf hydraulic conductance was experimentally determined on branches from 12 different mature individuals from each species. Terminal twigs of current year's growth were excised underwater and immediately fixed to tubing filled with 20mM KCl in distilled water in direct sunlight. While leaves transpired, the rate of water loss was recorded. Then a leaf was covered with foil and simultaneously cut with a sharp razor blade and bulk leaf xylem pressure measured in a pressure chamber. The leaf conductance was estimated as the transpirational rate divided by the leaf xylem pressure. Leaf area was measured using a leaf area meter (LI-COR 3100, Lincoln, Nebraska, USA). Hydraulic conductance was expressed per leaf area to give leaf-specific conductance *(K_L)*.

Tree parameters and growth rates

Height and diameter allometry was evaluated across trees of the size range used for the sapflow measures (see above; D=4-26 cm). We measured trunk diameter above the root crown (D) and maximum height (H) for all 36 sapflow trees as well as additional trees of the same size range (bigtooth maple N=64, Gambel oak N=51) in stands along the riparian corridor. Maximum tree height was measured with a clinometer, sighting to the topmost point on the tree canopy and then the height was geometrically calculated using the angle from the observer to the tree top and the observer's distance from the trunk. Mechanical constraints in mature trees dictate that trees grow according to elastic similarity. Elastic similarity prevents trees from growing too tall for a given diameter such that trees maintain a constant safety margin from buckling under their own weight. It has been shown theoretically and empirically that elastic similarity requires tree height (H) to scale with $D^{2/3}$ (Greenhill 1881, McMahon 1973, Niklas 1994, King 1986). Actual trees tend to become elastically similar as they grow from saplings to adult size (King 1986, Niklas 1995).

Wood density. Wood density was determined from the mean of six tree cores at breast height (~1 cm wide by 4 cm deep) and 6 branches (~ 4 cm long by 1 cm diameter) per species. Fresh volume was calculated from the weight of water displaced as wood samples were submerged in water on an electric balance (Archimedes principle). The segments were place in an 60° C oven for 14 days then removed and weighed again. Density was expressed as ρ= dry weight / fresh volume in g/cm^3.

Aboveground (shoot) mass. Tree height (H) by diameter (D) allometry combined with wood density measurements were used to determine shoot mass. By modeling trees as cylinders per DaVinci's rule (Richter 1970), we estimated the volume of each tree, or at least a proportional proxy for volume (V; $V= \pi/4\ D^2 H$). Combining tree volume with measurements of wood density (ρ, dry weight/fresh volume) yielded aboveground tree mass (M; $M=V\ \rho$) for each trunk diameter, D.

Leaf area. During August, fresh branches (diameter=0.14-1.38 cm) were gathered and stem cross-sectional area was measured and leaf area was measured using the leaf area meter (LI-COR 3100, Lincoln, Nebraska, USA). Leaves were then put in an oven at 60° C for 21 days. Then leaves were weighed resulting in a relationship of leaf area per leaf dry mass or specific leaf area (SLA). The fresh branches gave a relationship of leaf area per branch area (LA/BA) for each species. Assuming DaVinci's rule (trunk area=sum of stem areas), these branch-area-specific leaf areas were converted to leaf area per tree basal area for each experimental tree.

In homogeneous stands of each species, transects 50 m in length were selected running through the stand. During August, well before leaf drop, 5-gallon buckets were secured to the ground every 10 m for a total of 5 buckets per transect. At the end of the season, when all leaves had dropped, leaves were bagged, returned to lab and dried for another 14 days in the 60° C oven. All leaves from each bag were weighed for the total leaf area per bucket. Leaf area index (LAI; leave area per ground area), was estimated per species using the

SLA relationships from the fresh stems. Leaf area index was also measured over each bucket during August with a LAI instrument (LI-COR 2000, Lincoln, Nebraska, USA).

Shoot biomass growth rate (B). Aboveground biomass accumulation (B) was estimated from radial cores taken from trees at breast height. Trees were the same 36 individuals (18/species) used in sapflow measurements. Cores allowed us to reconstruct the relationship between diameter (D) and year for each tree. To reconstruct diameters for past years we incorporated bark thickness (measured from each tree core) allometric scaling from tree diameters. We converted D into mass (M) using the height allometry and wood density data. Then we obtained M vs. year relationships. From these data, the annual shoot biomass increments (B; B = ΔM/year) were estimated over the life of each experimental tree.

Statistical analyses. Numerous power functions were used to describe relationships between variables. These were obtained by linear regression through log-transformed data. Following the explicit advice of Warton et al. (2006), we used ordinary least squares (OLS) regression when the purpose was to predict a specific “y” value from a given “x” value. We used reduced major axis (RMA) regression when the purpose was to estimate the slope of the relationship (the scaling exponent). To analyze intraspecific differences in bigtooth maple and Gambel oak functions, homogeneity of regression slopes was performed in SPSS (SPSS, Inc. 1986, version 10). A standard t-test was used to test slopes and compare means between species.

Results

Water use in bigtooth maple and Gambel oak

During mid-summer periods of maximal transpiration, when soil moisture, light and VPD were not limiting, maximum daily sapflow (Q_{max}) scaled with tree diameter ($Q_{max} \propto D^q$) to an RMA regression exponent q=1.56 in bigtooth maple (95% confidence limit 1.24-1.88) and q=1.58 in Gambel oak (1.05-2.12; Fig. 2.1). The scaling exponent of less than q=2 means that larger trees used less water per basal area. Although the scaling exponents and intercepts were similar between species, bigtooth maple transported three to four times more water than Gambel oak across all tree diameters under conditions maximizing transpiration.

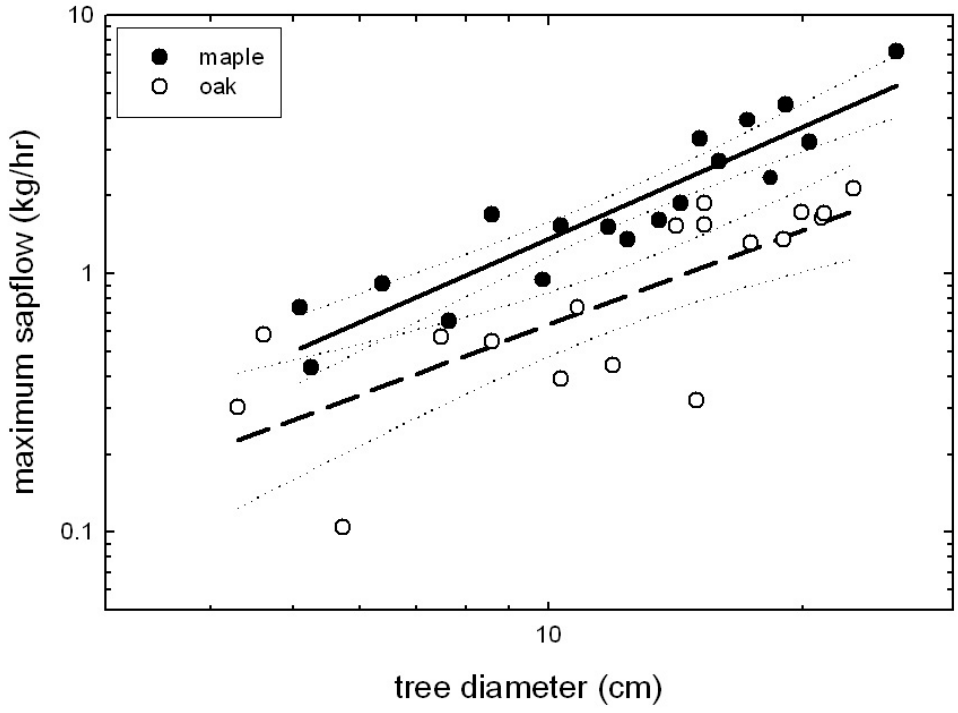

Figure 2.1. Relationship of maximum sapflow (Q_{max}) and tree diameter. The scaling exponent "q" for bigtooth maple =1.56 and for Gambel oak =1.58 (RMA regression). This relationship was used to correct for tree size and obtain standardize sapflow Q_s.

The average standardized daily sapflow ($Q_s = Q/D^q$) across all individuals per species showed that bigtooth maple transported more water than Gambel oak through most of the season (Fig. 2.2a). Water transport in bigtooth maple was initially low in the early summer due to a cool rainy period and then sapflow peaked during typical hot and dry conditions of mid-July. Gambel oak also had low sapflow in early summer followed by very consistent sapflow throughout the rest of mid- and late-summer. The relatively unvarying sapflow in Gambel oak was associated with stable or high (less negative) predawn water potentials suggesting deep rooting (Fig. 2.2b). At its maximum sapflow, bigtooth maple moved 2.5 times as much water per tree size as Gambel oak. As is common in this region, there were few precipitation events (bars in Figure 2.2a) during mid-summer. Bigtooth maple responded to drying soils with a decrease in sapflow and a significant decrease (regression line) in predawn water potentials suggesting shallow rooting (Fig. 2.2b). By the end of the season, bigtooth maple sapflow was near Gambel oak levels. Late in the season, after the first frost (maximum and minimum temperatures shown in dark and light grey respectively in Figure 2.2a) sapflow in both species dropped sharply with little sapflow thereafter.

To analyze cumulative seasonal water use, we chose the “cumulative growing season” (indicated by dotted vertical lines on Figure 2.2a) from the end of the cool rainy period (day 172) until the last frost-free day (day 272). On average, bigtooth maple moved 1.7 times more water than Gambel oak over the cumulative growing season. The maximum cumulative growing season sapflow

came from the largest bigtooth maple (diameter=31 cm) which moved 5,690 kg of water, while the largest Gambel oak (diameter=26 cm) moved 2,307 kg of water.

Bigtooth maple whole-tree conductance (standardized for tree size) averaged 1.7 times greater than Gambel oak with no seasonal trend (Fig. 2.2c). The outlier in bigtooth maple (day 184) was excluded from the seasonal trend analysis. It was associated with a 10 mm rain event the day before and low VPD values during the middle of the measurement day which may have prevented near-steady state conditions required for accurate conductance estimation. The lack of a significant decrease in whole-tree conductance through the season suggests that the sapflow decline in bigtooth maple was due to dropping soil-to-leaf pressure difference rather than a decrease in hydraulic conductance. Hydraulic resistance (inverse of conductance) was relatively evenly distributed between roots and shoots in bigtooth maple, while the majority (84%) of tree hydraulic resistance in Gambel oak was in the shoot (Fig. 2.3; Gambel oak=0.84 $\pm$ 0.03; bigtooth maple=0.57 $\pm$ 0.07).

Both species show response of sapflow to VPD throughout the entire measurement period (Fig. 2.4). Sapflow saturates at much lower VPD (1.5 KPa) in Gambel oak, suggesting more sensitive stomatal response. In bigtooth maple, sapflow rates continue to increase with increasing VPD, suggesting less sensitive stomatal response to VPD.

Various methods suggest that bigtooth maple and Gambel oak have similar leaf areas per tree size. Estimates of leaf area per trunk basal area

Figure 2.2. a) Size-normalized sapflow averaged across all trees per species (on left axis) versus day of year for bigtooth maple (solid circles) and Gambel oak (hollow circles). Maximum (dark grey line) and minimum (light grey line) daily temperatures and total daily precipitation (grey bars) versus day of year on right axis. Cumulative growing season (day 172-272; dotted vertical lines). b) Mean daily predawn (squares) and midday (triangles) water potentials for bigtooth maple (solid symbols) and Gambel oak (hollow symbols). Bigtooth maple showed a significant decreasing trend (regression line) in predawn water potentials. c) Standardized whole-tree conductance versus day of the year for bigtooth maple (solid circles) and Gambel oak (hollow circles).

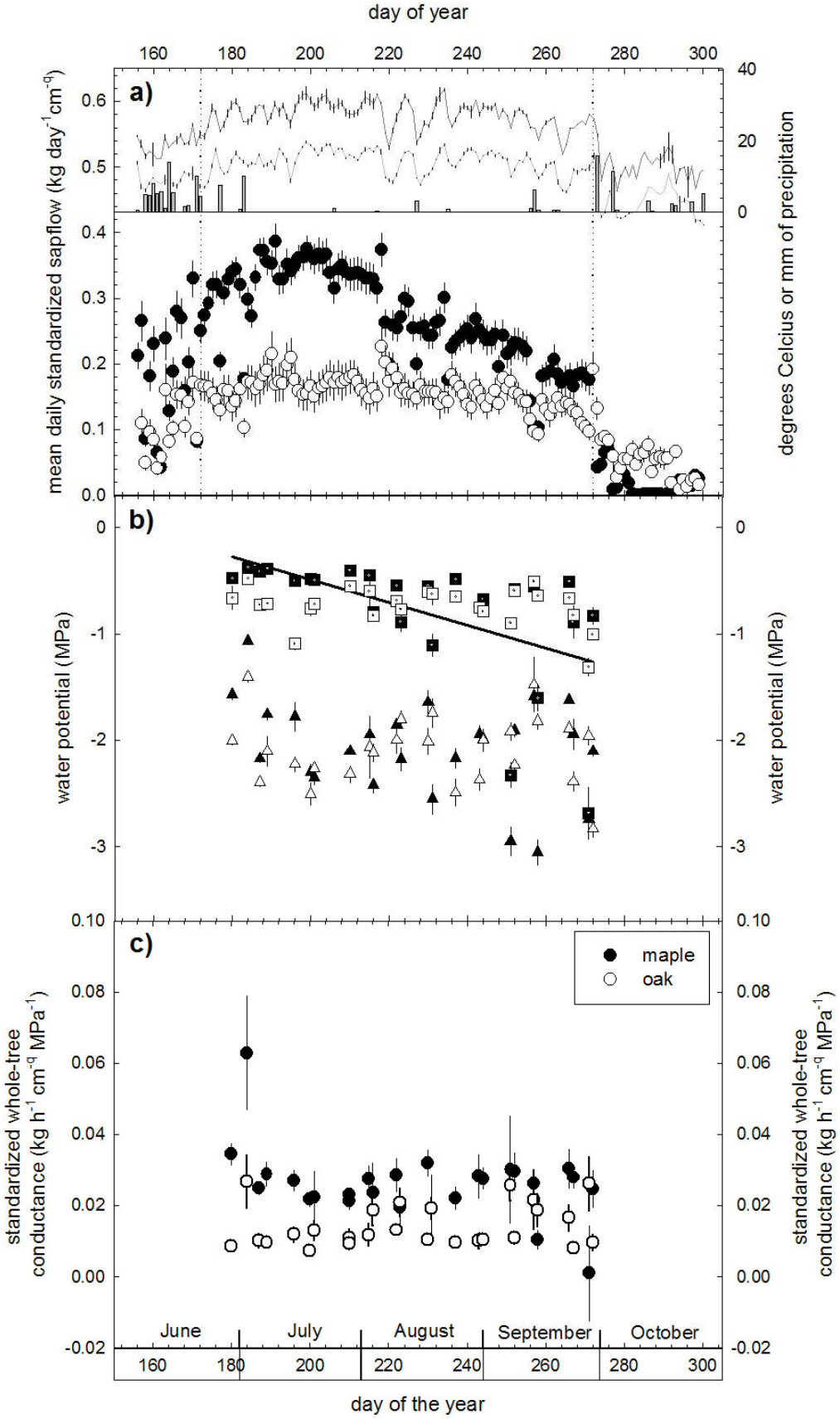
day of year
a)
b)
c)
mean daily standardized sapflow (kg day-1 cm-q)
degrees Celcius or mm of precipitation
water potential (MPa)
standardized whole-tree conductance (kg h-1 cm-q MPa-1)
maple
oak
June
July
August
September
October
day of the year

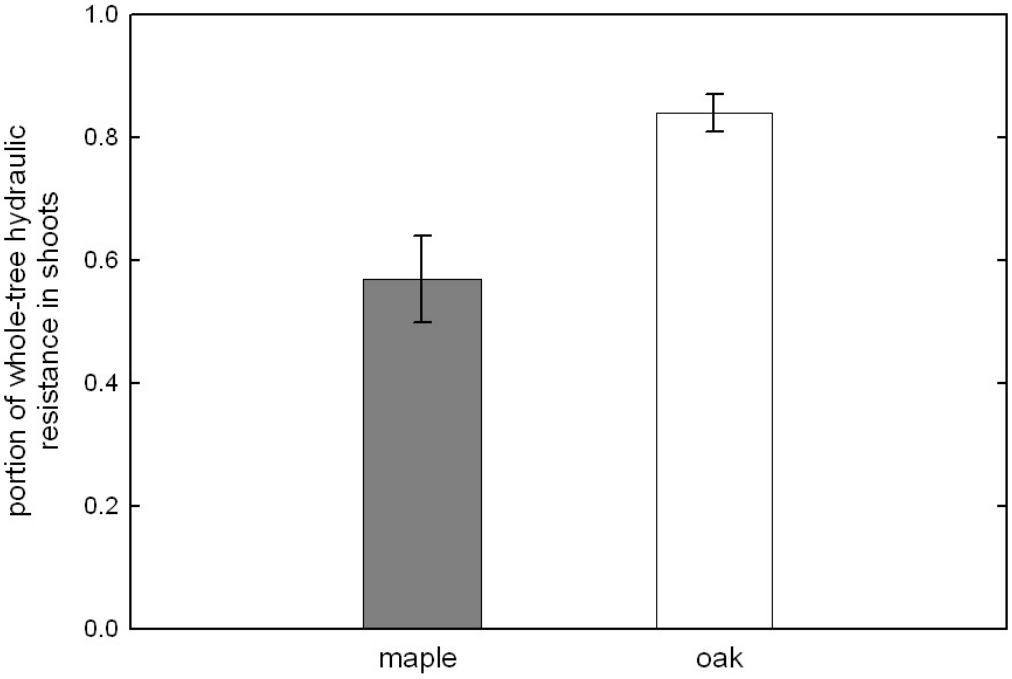

Figure 2.3. Mean portion of whole-tree hydraulic resistance in shoots for bigtooth maple (grey) and Gambel oak (white).

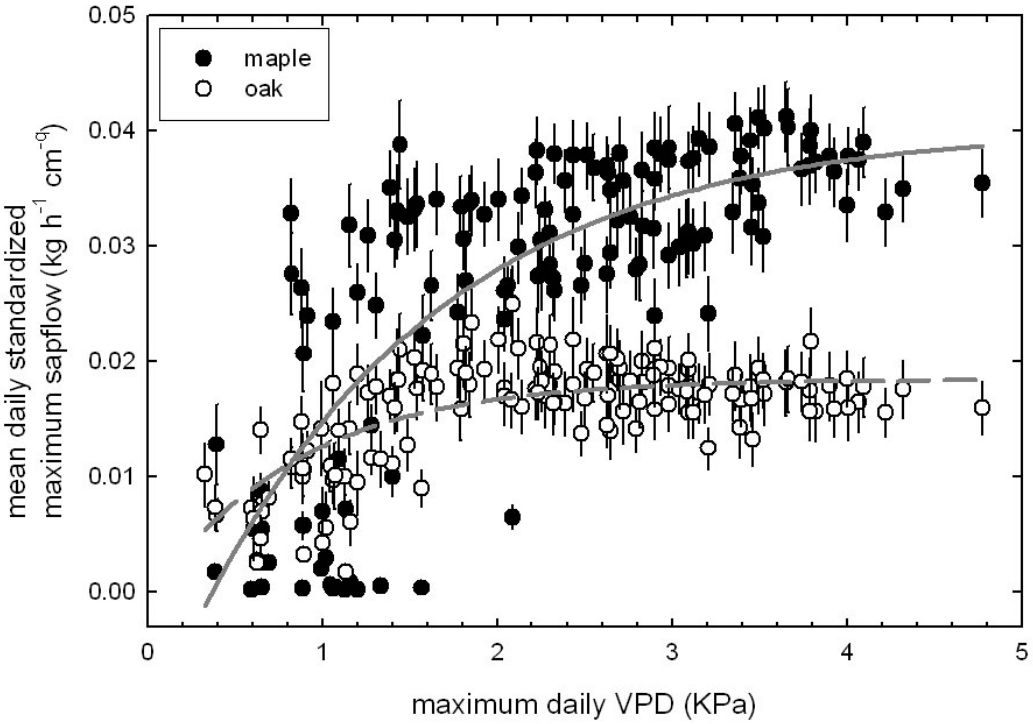

Figure 2.4. Daily standardized maximum sapflow averaged across individuals per species versus maximum daily VPD. Data were fit with exponential saturation curves (in grey; Q_{max} = a (1 - exp (b*VPD)).

showed similar results for bigtooth maple (759.0 ± 19.7) and Gambel oak (744.0 ± 32.6; Fig. 2.5). Specific leaf area (SLA) was significantly greater in bigtooth maple (127 ± 8 cm^2/g) than Gambel oak (100 ± 8 cm^2/g). Leaf area index (LAI) from LICOR LAI-2000 instrument showed bigtooth maple had 1.80 ± 0.12 LAI and Gambel oak had 1.97 ± 0.12. The bucket technique resulted in 4.75 ±0.38 LAI in bigtooth maple and 3.88 ±0.27 in Gambel oak. The measures of LAI area were limited in their utility because although measurements were made under monotypic stands the measurements were not easily corrected for tree diameter or total species basal area.

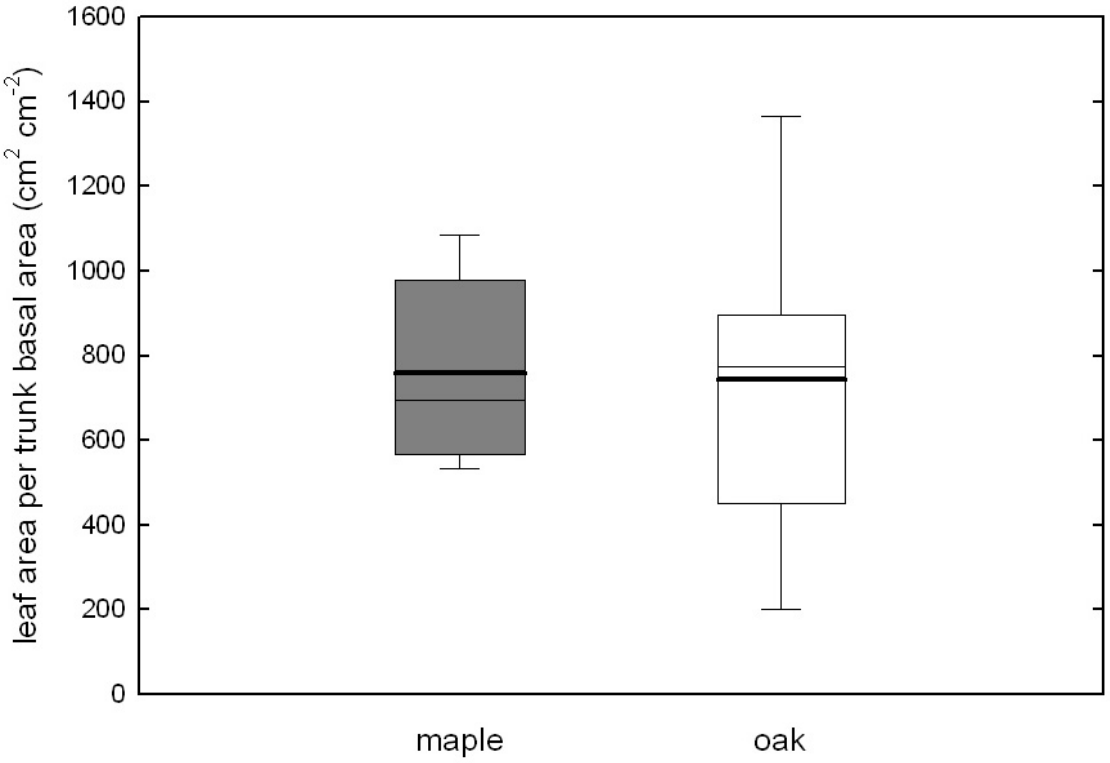

Figure 2.5. Mean leaf area per trunk area in bigtooth maple (grey) and Gambel oak (white). The heavy solid line within each box is the mean, the lighter line the median, the box the middle two quartiles (25-75 percentiles), and the bars the 10^{th} and 90^{th} percentile range.

Due to minimal sapwood area Gambel oak supports 52 times more leaf area per investment in sapwood area (LA/SA) than bigtooth maple (Gambel oak mean LA/SA=112 ± 15 m^2 cm^{-2}; bigtooth maple =2.13 ± .12 m^2 cm^{-2}). Gambel oak also had higher and more variable leaf hydraulic conductance per leaf area than bigtooth maple but the interspecific difference was not significant (Fig. 2.6; mean K_L in Gambel oak= 0.09 ± 0.023 mg s^{-1} KPa^{-1} m^{-2}; bigtooth maple =0.052 ± 0.005 mg s^{-1} KPa^{-1} m^{-2}).

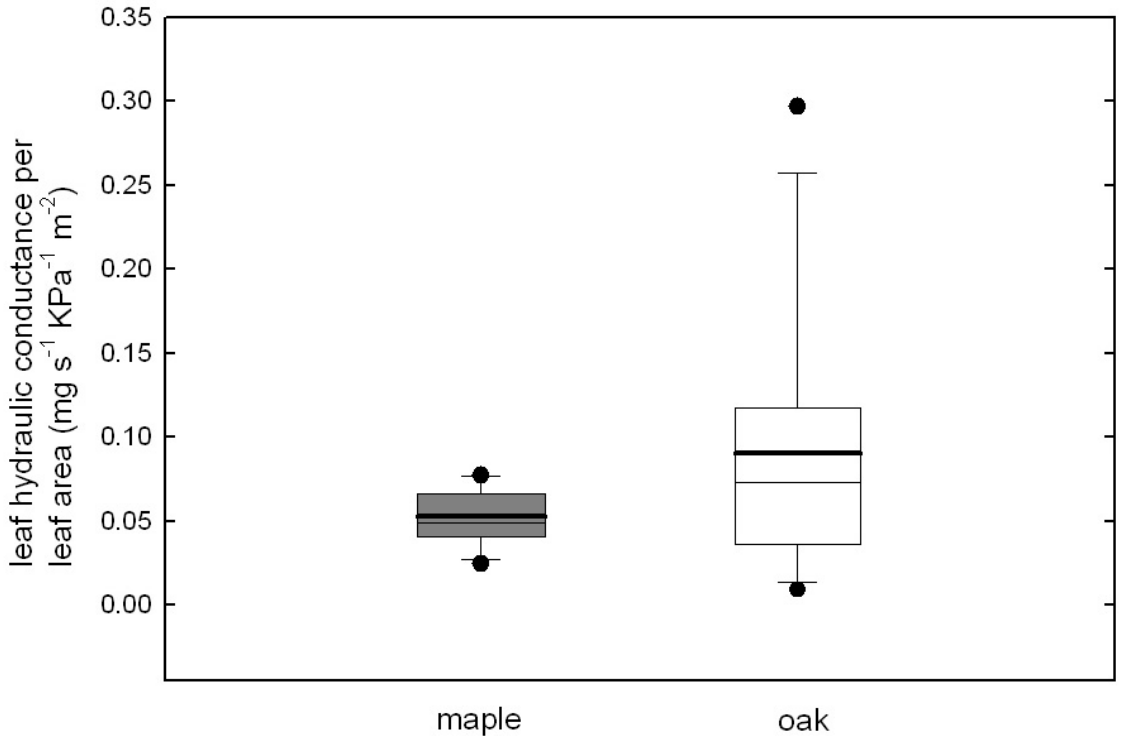

Figure 2.6. Mean leaf hydraulic conductance per leaf area in bigtooth maple (grey) and Gambel oak (white). The heavy solid line within each box is the mean, the lighter line the median, the box the middle two quartiles (25-75 percentiles), and the bars the 10th and 90th percentile range. Outliers are shown by solid symbols.

Tree parameters and growth rates in bigtooth maple and Gambel oak

Both species adhered to the mechanical constraints of elastic similarity with their height scaling with diameter to the 2/3 power (Fig. 2.7). Bigtooth maple scaling exponent (RMA) was 0.64 (95% confidence limit 0.57-0.71) and Gambel oak was 0.69 (0.59-0.80). Bigtooth maple reached a greater maximum height (bigtooth maple maximum height=18.3 m and Gambel oak=14.7 m) due to a smaller safety factor (SF) from buckling under its own weight than Gambel oak (bigtooth maple SF=2.61 ± 0.06; Gambel oak SF=3.38 ± 0.11). Both species had

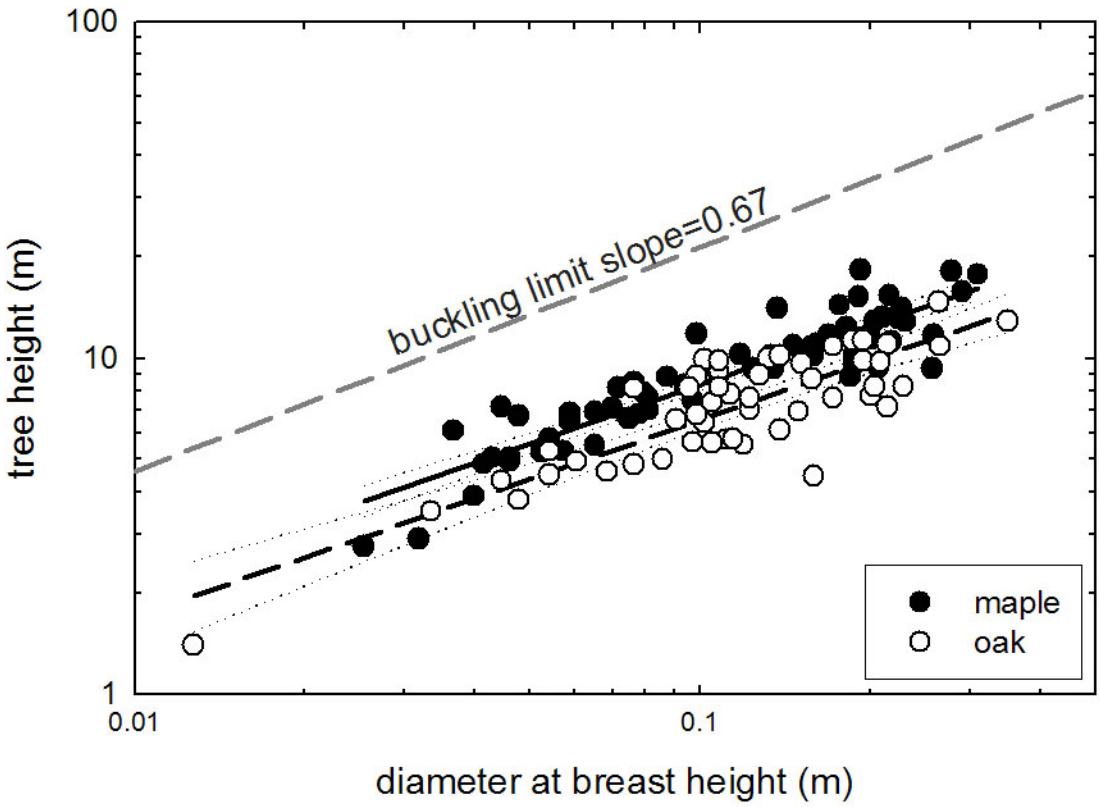

Figure 2.7. Tree height compared to diameter in bigtooth maple (solid circles) and Gambel oak (hollow circles). Both species were below the buckling limit (grey dotted line) indicating height at which tree would collapse under its own weight.

similar wood densities (bigtooth maple=0.637 $\pm$ 0.009 g/cm^3; Gambel oak=0.639 $\pm$ 0.012 g/cm^3).

Combining height and diameter scaling, DaVinci's rule, and wood density we estimated that shoot mass scaled similarly with diameter in both species($D \propto M^c$; bigtooth maple scaling exponent (RMA) c=0.39 (0.375-0.395), Gambel oak c=0.38 (0.367-0.399)). Shoot biomass growth rates from all rings at each tree core showed bigtooth maple had a greater log-linear regression slope of 2.09 (1.96-2.22; RMA) than Gambel oak with 1.83 (1.76-1.91; RMA), meaning bigtooth maple growth rates scale isometrically with basal area, while larger Gambel oak trees grow less per basal area (Fig. 2.8). Both the slopes and intercepts of these regressions were significantly different between species. Maple exhibited much greater year-to-year variation (R^2=0.36, oak R^2=0.77). The differences between species, though statistically significant, were minor and overall growth rates were of similar magnitude. During 2009, the year of sapflow measurement, the growth was not statistically different between species (exponents and intercepts not significantly different, Fig. 2.8, insert). During this year, bigtooth maple biomass growth scaled with diameter to the 1.60 (1.09-2.11; RMA) and Gambel oak scaling exponent was 1.79 (1.33-2.25; RMA).

Bigtooth maple biomass growth rates for 2009 scaled with 2009 cumulative growing season water use to the 0.87 (0.59-1.15; RMA) power compared to 1.06 (0.62-1.49; RMA) in Gambel oak. Scaling exponents and intercepts were not significantly different between species probably owing to Gambel oak's greater variability. However, the nonsignificant trend was for

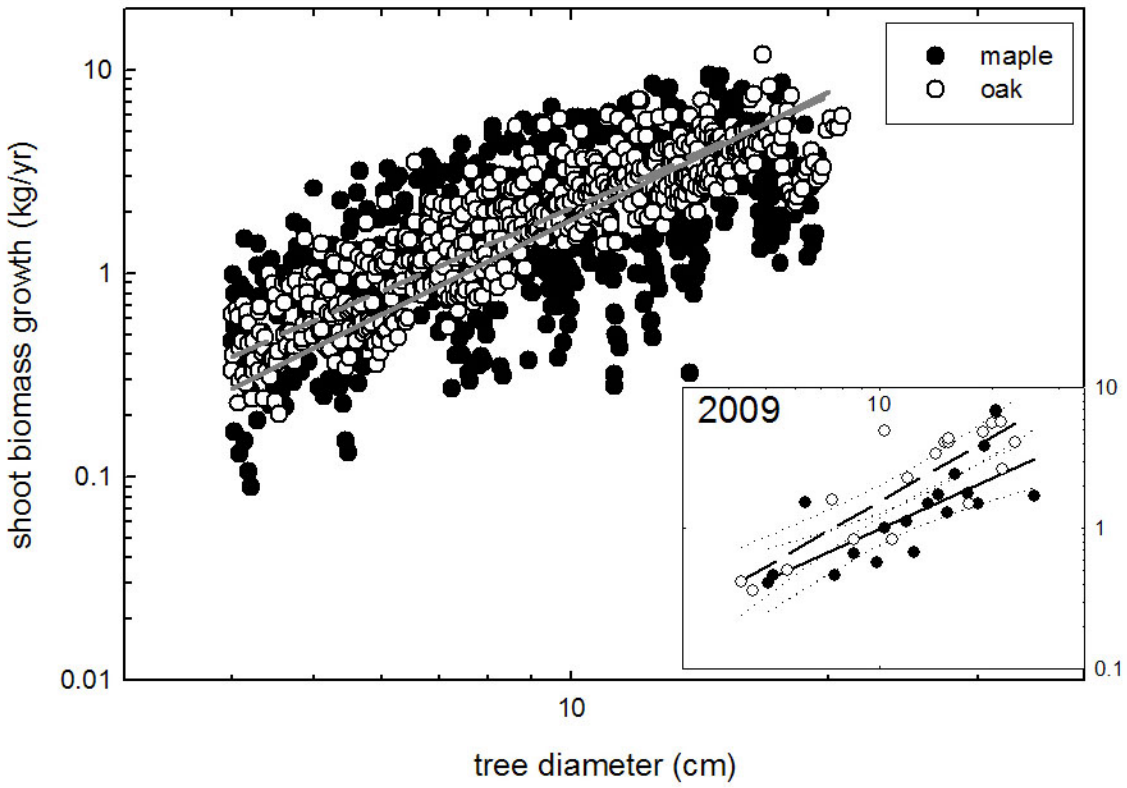

Figure 2.8. Shoot biomass growth rate from all rings and each tree core versus diameter in bigtooth maple (solid circles) and Gambel oak (hollow circles). The linear regressions are significantly different between maple (solid line) and oak (dashed line). Insert to right shows 2009 shoot biomass growth rates versus tree diameter.

Gambel oak to have 2.2 - 2.8 times higher shoot biomass growth rate per water use than bigtooth maple. This result suggests that Gambel oak makes more efficient use of water per investment in aboveground mass (Fig. 2.9). The mean ratio of water used per biomass growth rate from the 2009 cumulative growing season was 1221 ± 167 kg yr^{-1}/ kg yr^{-1} in bigtooth maple versus 451 ± 79 kg yr^{-1}/ kg yr^{-1} in Gambel oak.

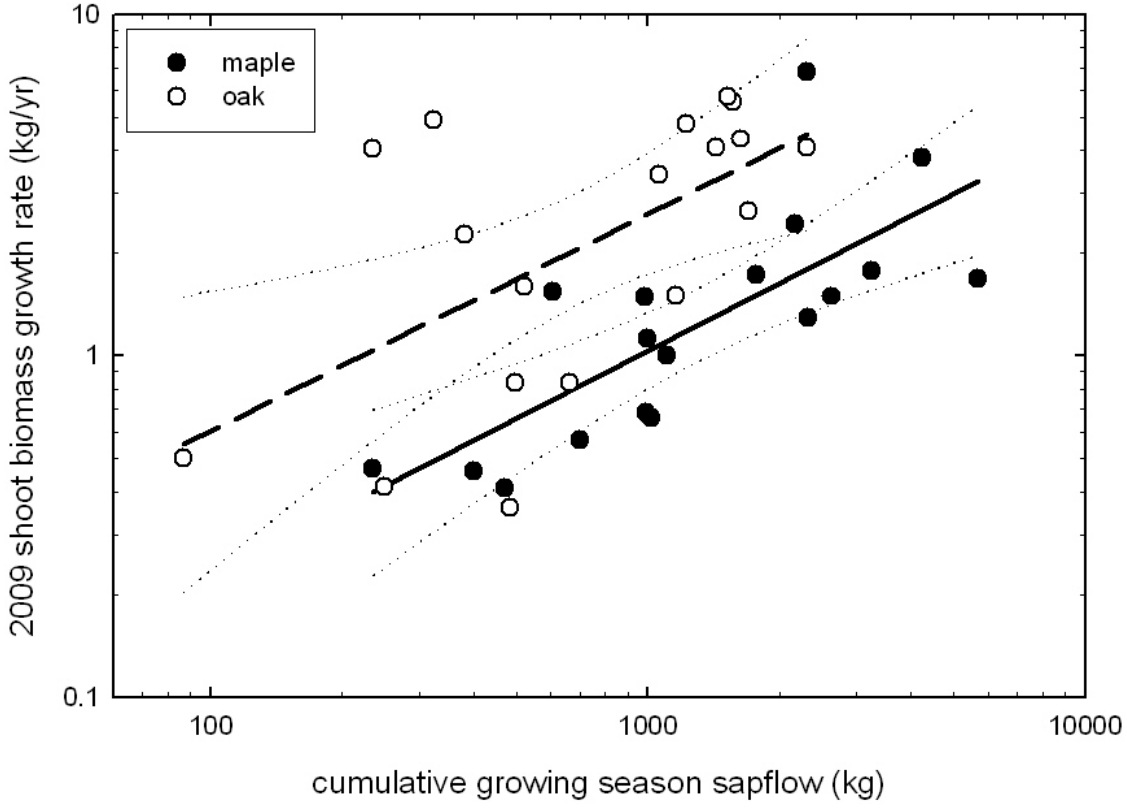

Figure 2.9. Shoot biomass growth rate for 2009 for each individual versus cumulative whole-tree sapflow across the cumulative growing season in bigtooth maple (solid circles) and Gambel oak (hollow circles).

Discussion

Bigtooth maple (*A. grandidientatum*) and Gambel oak (*Q. gambelii*) displayed very different hydraulic anatomy and water use behavior, yet achieved similar shoot growth rates. This is suggestive of being able to compete successfully in part by the exploitation of different water use strategies.

Gambel oak used roughly 40% less water than maple over the 100-day time frame analyzed, and exhibited roughly 40% lower size-specific hydraulic conductance (Fig. 2.2a, c). This moderate water use corresponded with high

stomatal sensitivity that maintained a VPD-invariant sapflow (Fig. 2.4), and a seasonally stable and high predawn xylem pressure indicative of deep roots (Fig. 2.2b). Gambel oak root systems had relative low hydraulic resistance (Fig. 2.3). These findings are consistent with other studies from the region that indicate isohydry and deep roots in Gambel oak (Taneda and Sperry 2008, Bush et al. 2008, Phillips and Ehleringer 1995, Williams and Ehleringer 2000, Ehleringer and Dawson 1992)).

An important result was that Gambel oak appeared to compensate for its lower water use with a 2- to 3-fold greater efficiency in converting water use to shoot biomass growth (Fig. 2.9). This efficiency is probably even greater than we report given that Gambel oak breaks bud a month later than bigtooth maple and has a consequently shorter growing season. In short, Gambel oak seems to offset its lower inherent conducting capacity by accessing a stable water source and using it efficiently.

Why are whole-tree sapflow and conductance so much lower in Gambel oak than bigtooth maple if Gambel oak has much larger vessels? Differences in water use and conductance oak can largely be explained by Gambel oak's wood anatomy. Like all ring-porous species, Gambel oak has a very low proportion of wood functioning as active sapwood per basal area (0.01 cm^2 cm^{-2} at basal diameter of 17 cm), while bigtooth maple has roughly 1/2 of its wood functioning as sapwood (0.46 cm^2 cm^{-2} at basal diameter of 17 cm). Although Gambel oak has much larger vessels and higher conductance capacity than bigtooth maple, this does not compensate for such minimal sapwood area. In addition, Taneda

and Sperry (2008) found that during a normal summer day (-1.5 MPa midday water potentials) a significant portion of the current year's earlywood vessels in Gambel oak were embolized. The embolized vessels appeared to refill overnight (at least early in the season) only to re-embolize the following day. Gambel oak branches at midday in that study averaged 1.8 times lower hydraulic conductivity per stem area (measured directly on stem segments) than bigtooth maple, supporting our similar finding at the whole-tree scale (whole-tree conductance in bigtooth maple was 1.7 times greater than Gambel oak). Although the theoretical hydraulic conductivity of an average earlywood oak vessel in the trunk (62 μm diameter) is equal to 45 times the hydraulic conductivity of maple's average trunk vessel (24 μm diameter), cavitation of these earlywood vessels results in a lower number of functional oak vessels resulting in lower conducting capacity per stem area.

Gambel oak had lower sapflow but similar leaf area compared with bigtooth maple (Fig. 2.5) implying that the oak has a lower canopy diffusive conductance to water vapor per leaf area. This assumption is consistent with an apparently greater sensitivity of Gambel oak stomata to VPD, as also observed in previous studies (Bush et al. 2008). Perhaps Gambel oak compensates for lower diffusive conductance with its lower specific leaf area (or thicker leaves) which may result in greater photosynthetic rate for a given diffusive conductance (Dijkstra 1989).

Lower water use per tree size in Gambel oak (Fig. 2.1) should result in less growth per tree size, but we found growth rates for 2009 not statistically

different from bigtooth maple in 2009 (Fig. 2.8, insert). Over the entire age distribution of the study trees, growth rates between the two species were also very similar (Fig. 2.8). These data indicate that Gambel oak is more efficient in exchanging water for shoot biomass growth, as was the trend in 2009. Different patterns of carbon allocation could explain Gambel oak's greater water use efficiency. For example, it is possible that the entire oak tree, roots plus shoots, does in fact put on less biomass growth than bigtooth maple, but that Gambel oak allocates a much greater annual portion to shoots than roots. There is much evidence that Gambel oak has relatively massive and deep roots that are long-lived. This is consistent with our finding that the Gambel oak root systems have much less hydraulic resistance than the shoots (Fig. 2.3). Perhaps relatively little annual root biomass is required to maintain this system (at least once it is established), making more of it available for shoot growth. Genet et al. (2010) found nine species of *Quercus* from temperate forests worldwide showed an exponential decrease in root to shoot biomass ratio with stand age until leveling off at 0.18 at roughly 90 years of age. Even the smaller trees measured in our study are likely connected to relatively large clonal root systems. Only trees grown from seedlings, which are rare in the region (Neilson and Wullstein 1983), would initially have to shunt more biomass to roots to establish a high root-shoot biomass ratio.

In addition, there is a tendency for leaf-level water use efficiency to increase with decreasing stomatal conductance (Donovan and Ehleringer 1994, Farquhar et al. 1989). The apparently lower canopy conductance in Gambel oak

may have increased its leaf-level water use efficiency, which in turn could have contributed to oak's greater whole-shoot water use efficiency that we observed (Fig. 2.9). More stable water status exhibited in Gambel oak may enhance photosynthetic efficiency and water use efficiency at the leaf level (Dina et al. 1973, Williams and Ehleringer 2000, Sanchez-Vilas and Retuerto 2007).

In contrast to Gambel oak, bigtooth maple's higher water use and conductance (Fig. 2.2a, c) corresponded with lower stomatal sensitivity lending to an increase in sapflow with increasing VPD (Fig. 2.4) despite low water potentials (Fig. 2.2b). The decreasing trend in predawn xylem potentials (Fig. 2.2b) did not lead to a significant decrease in hydraulic conductance over the season (Fig. 2.2c), indicating that there was little loss of conductance due to xylem cavitation in bigtooth maple. The sensitivity of bigtooth maple's water potential to decreasing soil moisture suggests shallow roots. This is consistent with other regional studies indicating anishohydry in bigtooth maple (Taneda and Sperry 2008, Bush et al. 2008, Phillips and Ehleringer 1995, Williams and Ehleringer 2000, Ehleringer and Dawson 1992). Anisohydric water status can lead to water stress (Franks et al. 2007). Bigtooth maple has been shown to endure periods of moderate drought stress due to cavitation-resistant xylem that can tolerate low water potentials (Taneda and Sperry 2008).

Bigtooth maple shows much more variability in growth rates than Gambel oak (Fig. 2.8). In this region with unpredictable summer precipitation, there should be more annual variation between growth rates and water use in anisohydric bigtooth maple. Bigtooth maple was more sensitive to soil moisture

stress presumably because of shallow roots and less strict stomatal control. Bigtooth maple's shallow roots allow for greater flexibility of resource use, yet the costly trade-off is greater vulnerablility to the deleterious effects of soil moisture deficit. In sites that are dry or during drier years, maple could suffer from drought stress and grow less than Gambel oak. Indeed, Figure 2.8 shows high variability in growth rates in shallow rooted bigtooth maple, while deep rooted Gambel oak showed much more consistent growth rates year to year. During 2009, Gambel oak had higher growth rates per tree size than bigtooth maple, perhaps due to little summer precipitation.

The lower water use efficiency in bigtooth maple is likely due in part to the costs of carbon allocation to surface roots that require development, maintenance and turn-over of fine roots and root hairs, and associations with symbiants. Alder et al. (1996) showed bigtooth maple surface roots had high rates of cavitation and turnover due to water stress. Conversely, after construction of deep roots, little maintenance and turnover occurs, meaning Gambel oak can allocate a greater percentage of its total carbon to shoot growth. Ehleringer and Dawson (1992) found that trees growing in habitats with low probability of summer rains have greater net carbon gain if they do not invest in fine roots but rather in deep roots. Our results support this concept with Gambel oak having deep roots and using water more efficient per growth rate than bigtooth maple with its dimorphic rooting habit. In addition, Gambel oak often sprouts new shoots from lignotubers (enlarged stem-like structure at the base of

the trunk). Perhaps these large established roots giving rise to new shoots can minimize the cost of deep root growth for clonal sprouts.

They key differences between these species are primarily due to their functional types (ring-porous and diffuse-porous) resulting in different approaches to hydraulics and carbon allocation. Ring-porous species have been shown to contain higher concentrations of total nonstructural carbohydrates than diffuse-porous species (Barbaroux and Brèda 2002, Genet et al. 2010). Ring-porous species accumulate more starch in their tissues while diffuse-porous species have been shown to accumulate more sugar (Barbaroux and Brèda 2002). Perhaps Gambel oak growth rates are more constant because oak uses carbon from the previous year for stem growth and vascular development before bud break (Barbaroux and Brèda 2002). Carbon invested into stem growth in ring-porous species is critical because the current year's ring is the extent of actively conducting sapwood for water transport. Diffuse-porous species are less dependent on the current year's growth for water transport, suggesting that diffuse-porous growth is more dependent on the current year's resources availability. Diffuse-porous species have been shown to decrease carbon allocated to growth rates in order to bolster reproduction and storage for longevity (Genet et al. 2010).

In summary, we found ring-porous Gambel oak to be less sensitive to water stress and more dependent on stable water sources enabling stable and efficient carbon fixation. Diffuse-porous bigtooth maple was more flexible in resource use yet more sensitive to water stress due to dependence on surface

soil moisture leading to fluctuations in carbon fixation rates. Overall the growth strategy we observed in Gambel oak agrees with findings of Genet et al. (2010) showing that ring-porous *Quercus* species have more stable growth rates year to year. These findings lead Genet et al. (2010) to propose that ring-porous *Quercus* species are less flexible to perturbations of the environment than diffuse-porous *Fagus* species. Perhaps this helps to explain the lower diversity and more limited distribution of ring-porous species worldwide than more flexible diffuse-porous species.

We found interesting similarities and differences in bigtooth maple and Gambel oak enabling their coexistence in the Intermountain West region. Notably both species adhere to mechanical constraints, developing their external structure in similar and predictable ways, lending to similar scaling of size with water use and growth rates. However, due to their divergent internal hydraulic architecture, these two species partition water resources into separate spatial and temporal niches. These two species are competitive in a riparian habitat by being good at different things. Isohydric water use allows Gambel oak to be less prone to water stress by accessing a stable water source and tightly regulating stomata. In contrast, anisohydric water use makes bigtooth maple good at early season water consumption with growth rates that are sensitive to inter-annual variability in water stress. In summary, bigtooth maple is better at moving water for a given tree size, while Gambel oak is more efficient at converting a unit of water into shoot biomass growth.

Literature Cited

Alder, N. N., J. S. Sperry, and W. T. Pockman. 1996. Root and stem xylem embolism, stomatal conductance, and leaf turgor in *Acer grandidentatum* populations along a soil moisture gradient. Oecologia **105**:293-301.

Barbaroux, C. and N. Brèda. 2002. Contrasting distribution and seasonal dynamics of carbohydrate reserves in stem wood of adult ring-porous sessile oak and diffuse-porous beech trees. Tree Physiology **22**:1201-1210.

Bush, S. E., K. R. Hultine, J. S. Sperry, and J. R. Ehleringer. 2010. Calibration of thermal dissipation sap flow probes for ring- and diffuse-porous trees. Tree Physiology **30**:1545-1554.

Bush, S. E., D. E. Pataki, K. R. Hultine, A. G. West, J. S. Sperry, and J. R. Ehleringer. 2008. Wood anatomy constrains stomatal responses to atmospheric vapor pressure deficit in irrigated, urban trees. Oecologia **156**:13-20.

Crow, T. R. 1978. Common regressions to estimate tree biomass in tropical stands. Forest Science **24**:110-114.

Davis, S. D., J. S. Sperry, and U. G. Hacke. 1999. The relationship between xylem conduit diameter and cavitation caused by freeze-thaw events. American Journal of Botany **86**:1367-1372.

Dijkstra, P. 1989. Cause and effect of differences in specific leaf area. Cause and consequences of variation in growth rate and productivity of higher plants 125-141.

Dina, S. J., L. G. Klickoff, and M. B. Keddington. 1973. Seasonal water potential patterns in mountain brush zone, Utah. American Midland Naturalist **89**:70-80.

Dobrowolski, J. P., M. M. Caldwell, and J. H. Richards. 1990. Basin hydrology and plant root systems. Pages 243-292 *in* C. B. Osmond, L. F. Pitelka, and G. M. Hidy, editors. Plant Biology of the Basin and Range. Springer-Verlag, Berlin.

Donovan, L. E., JR. 1994. Carbon isotope discrimination, water-use efficiency, growth, and mortality in a natural shrub population. Oecologia **100**:347-354.

Ehleringer, J. R., L. A. Arnow, T. Arnow, I. B. McNulty, and N. C. Negus. 1992. Red Butte Canyon Research Natural Area: history, flora, geology, climate, and ecology. Great Basin Naturalist **52**:95-121.

Ehleringer, J. R. and T. E. Dawson. 1992. Water uptake by plants: perspectives from stable isotopes. Plant Cell and Environment **15**:1073-1082.

Ellmore, G. S. and F. W. Ewers. 1986. Fluid flow in the outermost xylem increment of a ring-porous tree, *Ulmus americana*. American Journal of Botany **73**:1771-1774.

Engle, D. M., C. D. Bonham, and L. E. Bartel. 1983. Ecological characteristics and control of Gambel oak. Journal of Range Management **36**:363-365.

Franks, P. J., P. L. Drake, and R. H. Froend. 2007. Anisohydric but isohydrodynamic: seasonally constant plant water potential gradient explained by a stomatal control mechanism incorporating variable plant hydraulic conductance. Plant Cell and Environment **30**:19-30.

Farquhar, G. D., J. R. Ehleringer, and K. T. Hubick. 1989. Carbon isotope discrimination and photosynthesis. Annual Review of Plant Physiology and Plant Molecular Biology **40**:503-537.

Genet, H., N. Brèda, and E. Dufrêne. 2010. Age-related variation in carbon allocation at tree and stand scales in beech (*Fagus sylvatica* L.) and sessile oak (*Quercus petraea* (Matt.) Liebl.) using a chronosequence approach. Tree Physiology **30**:177-192.

Granier, A. 1985. Une nouvelle methode pour la mesure du flux de seve brute dans le tronc des arbes. Annales des Sciences Forestieres **42**:193-200.

Greenhill, A. G. 1881. Determination of the greatest height consistent with stability that a vertical pole or mast can be made, and the greatest height to which a tree of given proportions can grow. Proceedings of the Cambridge Philosophical Society.

Hacke, U. and J. J. Sauter. 1996. Xylem dysfunction during winter and recovery of hydraulic conductivity in diffuse-porous and ring-porous trees. Oecologia **105**:435-439.

Hacke, U. G., J. S. Sperry, J. K. Wheeler, and L. Castro. 2006. Scaling of angiosperm xylem structure with safety and efficiency. Tree Physiology **26**:689-701.

King, D. A. 1986. Tree form, height growth, and susceptibility to wind damage in *Acer saccharum*. Ecology **67**:980-990.

Lechowicz, M. J. 1984. Why do temperate deciduous trees leaf out when they do? Adaptation and the ecology of forest communities. American Naturalist **124**:821-842.

McMahon, T. A. 1973. Size and shape in biology. Science **179**:1201-1204.

Neilson, R. P. and L. H. Wullstein. 1983. Biogeography of two southwest American oaks in relation to atmospheric dynamics. Journal of Biogeography **10**:275-297.

Neilson, R. P. and L. H. Wullstein. 1985. Comparative drought physiology and biogeography of *Quercus gambelii* and *Quercus turbinella*. The American Midland Naturalist **114**:259-271.

Niklas, K. J. 1994. The allometry of safety-factors for plant height. American Journal of Botany **81**:345-351.

Phillips, S. L. and J. R. Ehleringer. 1995. Limited uptake of summer precipitation by bigtooth maple (*Acer grandidentatum* Nutt) and Gambel oak (*Quercus gambelii* Nutt). Trees-Structure and Function **9**:214-219.

Richter, J. P. 1970. The notebooks of Leonardo da Vinci (1452-1519), compiled and edited from the original manuscripts. Dover, New York.

Sanchez-Vilas, J. and R. Retuerto. 2007. *Quercus ilex* shows significant among-population variability in functional and growth traits but maintains invariant scaling relations in biomass allocation. International Journal of Plant Sciences **168**:973-983.

Sperry, J. S. and J. E. M. Sullivan. 1992. Xylem embolism in response to freeze-thaw cycles and water stress in ring-porous, diffuse-porous, and conifer species. Plant Physiology **100**:605-613.

Taneda, H. and J. S. Sperry. 2008. A case-study of water transport in co-occurring ring- versus diffuse-porous treses: contrasts in water-status, conducting capacity, cavitation and vessel refilling. Tree Physiology **28**:1641-1652.

Tiedemann, A. R., W. P. Clary, and R. J. Barbour. 1987. Underground systems of Gambel oak (*Quercus gamelii*) in central Utah. American Journal of Botany **74**:1065-1071.

Wang, J., N. E. Ives, and M. J. Lechowicz. 1992. The relation of foliar phenology to xylem embolism in trees. Functional Ecology **6**:469-475.

Williams, D. G. and J. R. Ehleringer. 2000. Intra- and interspecific variation for summer precipitation use in pinyon-juniper woodlands. Ecological Monographs **70**:517-537.

Wilson, K. B., P. J. Hanson, P. J. Mulholland, D. D. Baldocchi, and S. D. Wullschleger. 2001. A comparison of methods for determining forest evapotranspiration and its components: sap-flow, soil water budget, eddy covariance and catchment water balance. Agricultural and Forest Meteorology **106**:153-168.

Zimmermann, M. H. 1983. Xylem structure and the ascent of sap. Springer, Berlin Heidelberg New York.

Zimmermann, M. H. and C. L. Brown. 1971. Trees: Structure and function. Springer-Verlag, Berlin.